A survey of molecular gas in luminous sub-millimetre galaxies

M. S. Bothwell,[1,2]⋆ Ian Smail,[3] S. C. Chapman,[2] R. Genzel,[4] R. J. Ivison,[5,6] L. J. Tacconi,[4] S. Alaghband-Zadeh,[2] F. Bertoldi,[7] A. W. Blain,[8] C. M. Casey,[9] P. Cox,[10] T. R. Greve,[11] D. Lutz,[4] R. Neri,[10] A. Omont[12] and A. M. Swinbank[3]

[1]*Steward Observatory, University of Arizona, Tucson, AZ 85721, USA*
[2]*Institute of Astronomy, University of Cambridge, Cambridge CB3 0HA, UK*
[3]*Institute for Computational Cosmology, Durham University, Durham DH1 3LE, UK*
[4]*Max-Planck-Institut für extraterrestrische Physik, Postfach 1312, D-85741 Garching, Germany*
[5]*UK Astronomy Technology Centre, Royal Observatory, Blackford Hill, Edinburgh EH9 3HJ, UK*
[6]*Institute for Astronomy, University of Edinburgh, Blackford Hill, Edinburgh EH9 3HJ, UK*
[7]*Argelander-Institut für Astronomie, Auf dem Hügel 71, D-53121 Bonn, Germany*
[8]*Department of Physics and Astronomy, University of Leicester, University Road, Leicester, LE1 7RH, UK*
[9]*Institute for Astronomy, University of Hawaii, 2680 Woodlawn Drive, Honolulu, HI 96822, USA*
[10]*Institut de Radio Astronomie Millimetrique (IRAM), Saint Martin d'Heres, France*
[11]*Department of Physics and Astronomy, University College London, Gower Street, WC1E 6BT, UK*
[12]*CNRS and Institut d'Astrophysique de Paris, 98 bis boulevard Arago, F-75014 Paris, France*

ABSTRACT

We present the results from a survey of ^{12}CO emission in 40 luminous sub-millimetre galaxies (SMGs), with 850-μm fluxes of $S_{850\,\mu m} = 4$–20 mJy, conducted with the Plateau de Bure Interferometer. We detect ^{12}CO emission in 32 SMGs at $z \sim 1.2$–4.1, including 16 SMGs not previously published. Using multiple ^{12}CO line ($J_{up} = 2$–7) observations, we derive a median spectral line energy distribution for luminous SMGs. We report the discovery of a fundamental relationship between ^{12}CO FWHM and ^{12}CO line luminosity in high-redshift starbursts, which we interpret as a natural consequence of the baryon-dominated dynamics within the regions probed by our observations. We use far-infrared luminosities to assess the star formation efficiency in our SMGs, finding that the slope of the L'_{CO}–L_{FIR} relation is close to linear. We derive molecular gas masses, finding a mean gas mass of $(5.3 \pm 1.0) \times 10^{10}$ M$_\odot$. Combining these with dynamical masses, we determine the redshift evolution of the gas content of SMGs, finding that they do not appear to be significantly more gas rich than less vigorously star-forming galaxies at high redshifts. Finally, we collate X-ray observations, and study the interdependence of gas and dynamical properties of SMGs with their AGN activity and supermassive black hole masses (M_{BH}), finding that SMGs lie significantly below the local M_{BH}–σ relation.

Key words: galaxies: evolution – galaxies: formation – galaxies: ISM – cosmology: observations.

1 INTRODUCTION

The discovery of a population of sub-millimetre (sub-mm) bright, highly star-forming galaxies (SMGs) at high redshift has provided a critical challenge for hierarchical galaxy evolution models (Blain et al. 1999; Baugh et al. 2005). These luminous 'sub-mm galaxies' (SMGs) are young, highly dust obscured galaxies, at a median $\langle z \rangle > \sim 2.5$ (e.g. Chapman et al. 2003, 2005 (hereafter C05); Ward-

low et al. 2011), with extreme far-infrared (far-IR) luminosities ($L_{FIR} = 10^{12}$–10^{13} L$_\odot$) implying prodigious star formation rates (SFRs) of $\gtrsim 10^3$ M$_\odot$ yr^{-1} (Chapman et al. 2010; Magnelli et al. 2012). As they are selected at 850 μm (corresponding to rest frame $\lambda \sim 200$–400 μm) these sources tend to have significant masses of cold dust (C05, see also Magnelli et al. 2012), as well as correspondingly substantial reservoirs of molecular gas ($\sim 10^{10}$ M$_\odot$; Greve et al. 2005). Together with their high stellar masses ($\sim 10^{11}$ M$_\odot$; e.g. Hainline et al. 2011) this suggests this population reside in some of most massive dark matter haloes in the high-redshift Universe.

⋆ E-mail: matthew.bothwell@gmail.com

SMGs have been studied extensively since their discovery in the 850-μm atmospheric window using the Submillimetre Common User Bolometer Array (SCUBA; Holland et al. 1999) on the JCMT (Smail, Ivison & Blain 1997), and it is clear that they represent a population of cosmological importance. Recent advances in IR-detector technology have opened up the possibility of much wider field surveys at these wavelengths, including *Herschel* SPIRE at 500 μm (Chapman et al. 2010; Magnelli et al. 2010, 2012), in the millimetre waveband with the South Pole Telescope (Vieira et al. 2010) and surveys with the new SCUBA-2 camera (Holland et al., in preparation) on JCMT. These surveys are providing large numbers of dusty galaxies with properties similar to the original SCUBA population. In this work, we use the term 'SMG' to refer to 850-μm-selected galaxies which comprise the bulk of our sample.

SMGs are defined as sub-mm sources with fluxes of $\gtrsim 1$ mJy at 850 μm, corresponding to $L_{FIR} \gtrsim 10^{12}$ L$_\odot$ (ULIRGs). Some authors have defined a 'main sequence' of star formation (defined as SFR/$M_* \sim M_*^\alpha (1 + z)^\beta$; Daddi et al. 2007; Noeske et al. 2007; Schiminovich et al. 2007; Rodighiero et al. 2010). SMGs typically lie ~ 1 dex above this 'main sequence', significantly more than the scatter around the sequence, which is typically $\sim \pm 0.3$ dex.

Due to a range of kinematic and morphological evidence, many authors have argued that SMGs can be understood as 'scaled-up' analogues of ultraluminous IR galaxies (ULIRGs) in the local Universe, which typically lie an order of magnitude (or more) above the SFR–$M_\star$ 'main sequence' (Tacconi et al. 2006, 2008; Engel et al. 2010). In this picture, luminous SMGs are best understood as major-merger events, with the extreme star formation being driven by the merger.

There have also been claims, however, for a secular origin for some SMGs. Theoretical simulations that model SMGs as massive, star-forming discs reproduce some of the physical properties of the SMG population, while avoiding some of the possible difficulties that arise from ascribing a merger origin to all SMGs (such as the observed number counts). While there has been some corroborating evidence for this picture (e.g. Bothwell et al. 2010 presented evidence for a luminous SMG with disc-like properties), simulated disc-like SMGs generally fail to reproduce the extreme SFRs characteristic of the bright end of the SMG population.

Some sub-mm sources may also be formed by the unresolved emission from a number of less luminous galaxies. High-resolution imaging has resolved a few sub-mm sources into two (or more) less luminous SMGs, which happen to fall within the same sub-mm detection beam, pushing the combined system above the SMG survey detection limits (see Wang et al. 2011; Barger et al. 2012; Karim et al. 2012). In addition, Chapman et al. (2002), C05 and Banerji et al. (2011) confirmed the presence of a population of lower luminosity galaxies at lower redshifts, which are selected at sub-mm wavelengths due to unusually cold dust temperatures. An overarching theme of the results over the last few years has therefore been an appreciation of the diversity of the SMG population. The transition between the brightest starburst sources and the more secular systems is undoubtably a gradual one, and it is likely that a mix of models is required if we are to fully understand the entirety of the SMG population.

Observations of the cold molecular phase of the interstellar medium (ISM) have the power to resolve many of these issues, as well as providing unique insight into the physics and behaviour of these systems. Molecular line observations provide the most direct insight into galaxy dynamics (e.g. Walter, Carilli & Daddi 2011) with turbulent merging systems having very different kinematic profiles from ordered rotating discs (Neri et al. 2003; Tacconi et al. 2006, 2008, 2010). In addition, molecular gas linewidths provide excellent estimates of the dynamical mass of galaxies, free from the uncertainties (extinction effects and non-gravitational motions, such as winds) that can potentially affect estimates derived from optical and near-IR observations.

From the intensity of the observed ^{12}CO emission lines, it is possible to calculate the mass of the molecular gas reservoir. As molecular hydrogen lacks a permanent electric dipole, it is all but invisible for even nearby galaxies. Instead, ^{12}CO is used as a tracer molecule, as it is produced in similar conditions to molecular hydrogen and is collisionally thermalized by H$_2$ even at low densities (though it is typically optically thick). Once the relative ratio of ^{12}CO luminosity to H$_2$ mass is known (the conversion factor is usually parametrized as α), it is possible to calculate the mass of the underlying H$_2$ reservoir. When combined with far-IR luminosities (calculated directly, or inferred from radio continuum flux observations via the far-IR/radio correlation), gas masses provide estimates of the star formation efficiencies (SFE) in SMGs (e.g. Greve et al. 2005; Daddi et al. 2010; Genzel et al. 2010). Whether such extreme starburst galaxies have similar SFE to more 'normal' SMGs at similar epochs, or whether modification is needed in order to explain their prodigious SFRs, has important implications for galaxy evolution models.

Historically, a number of instrumental limitations have caused molecular gas in high-redshift galaxies to be poorly studied. Observing molecular gas is very time consuming with current instrumentation, with on-source integration times of several hours being typical for even luminous ^{12}CO sources. In addition, several steps are required in order to observe a ^{12}CO line once an SMG has been detected at sub-mm wavelengths. After the galaxy has been detected with the typically low-resolution sub-mm or far-IR beam, an accurate position is required using radio continuum emission (Biggs et al. 2011; Ivison et al. 2001). Only then can UV spectroscopy obtain an accurate redshift (C05), and only at that point could the relatively narrow-bandwidth receivers observe ^{12}CO transitions. Of course, with the higher resolution imaging in the far-IR/sub-mm made available by the advent of Atacama Large Millimeter/submillimeter Array (ALMA), the positioning of SMG-bright sources is becoming easier, and with increased bandwidths available at mm wavelengths the required redshift accuracy is now becoming less of an issue.

One significant weakness of the studies of the gas content of high-redshift starbursts published to date is their poor redshift coverage, and subsequent limited ability to address evolutionary effects in the molecular gas properties of SMGs. The redshift evolution of molecular gas fractions and dynamical masses encodes important information relating to the assembly of massive galaxies, providing valuable constraints on models of structure formation.

In view of the importance of this population, and of the paucity of existing data sets, we undertook a large survey for ^{12}CO emission in a large sample of SMGs using the IRAM Plateau de Bure Interferometer (PdBI), aiming to draw significant conclusions about the SMG population as a whole across a wide range of redshifts. This makes it possible, for the first time, to address evolutionary effects in the gas properties of luminous SMGs.

Our IRAM PdBI SMG survey was started in 2002. Prior to the start of the survey, only two SMGs had been detected in ^{12}CO, SMM J02399−0136 ($z = 2.81$; Frayer et al. 1998; Ivison et al. 1998; Genzel et al. 2003) and SMM J14011+0252 ($z = 2.56$; Frayer et al. 1999; Ivison et al. 2001). The first results from the PdBI SMG survey were published by Neri et al. (2003) and Greve et al.

(2005), who added ^{12}CO detections of three and five new SMGs, respectively. In addition, spatially resolved (sub-arcsecond) imaging for a total of 12 SMGs from the survey has been reported by Tacconi et al. (2006, 2008), Bothwell et al. (2010) and Engel et al. (2010). The IRAM PdBI SMGs survey has now reached its conclusion observations of 40 SMGs at $z \sim 1$–4 observed in a range of ^{12}CO transitions.

In Section 2, we give details of the survey, the observing strategy used and the reduction and analysis of the data. Section 3 presents a median spectral line energy distribution (SLED) for the sample, from which luminosity ratios are estimated. In Section 4, we describe the physical properties of the SMG sample as revealed by the ^{12}CO observations, including the kinematic properties, dynamical masses, SFE and molecular gas properties. In Section 4.6, we also compare baryonic and dynamical mass measurements, and discuss the implications for deriving physically motivated parameters for SMGs. Section 5 then discusses the effects of supermassive black hole (SMBH) activity on the SMG population, and Section 6 presents our conclusions.

Throughout this work, we adopt a cosmological model with $(\Omega_m, \Omega_\Lambda, H_0) = (0.27, 0.73, 71 \text{ km s}^{-1} \text{ Mpc}^{-1})$, and a Chabrier (2003) IMF.

2 OBSERVATIONS, REDUCTION AND SAMPLE PROPERTIES

2.1 Sample selection

Our full sample of SMGs observed with the PdBI low-resolution programme consists of 40 galaxies[1] at $z \sim 1$–4. The initial target selection was drawn from the optical-spectroscopic survey of SMGs by C05, as well as the SCUBA Cluster Lens Survey (Smail et al. 2002) and the SCUBA Half Degree Extragalactic Survey (SHADES) of the Subaru/*XMM–Newton* Deep Field (Coppin et al. 2006). Given the duration of the survey, our observing strategy naturally evolved with time, taking advantage of the rapid advance of other multiwavelength projects studying this population. Therefore, as the survey progressed we also included a few of the first spectroscopically identified millimetre-selected galaxies (from surveys with the MAMBO camera on the IRAM 30 m; Bertoldi et al. 2002; Greve et al. 2004), as well as SMGs with more precise rest-frame optical redshifts derived from near- or mid-IR spectroscopy. As a result the final target sample includes SMGs selected to have precise spectroscopic redshifts, derived using one or more of the following techniques: (i) Lyman α emission (C05); (ii) Hα emission (Swinbank et al. 2004) and (iii) polycyclic aromatic hydrocarbon emission from mid-IR spectroscopy with *Spitzer* (Pope et al. 2008; Menéndez-Delmestre et al. 2009).

For those SMGs with only optical (rest-frame UV) spectroscopy at the time of observation, we used the median velocity offset between optical and near-IR redshifts for SMGs to estimate the likely velocity offsets of their systemic redshift from the optically derived value. The resulting redshift uncertainty is $\Delta z = 0.005$ and this should guarantee that the ^{12}CO emission from an SMG at $z \geq 1$ would fall within the 580-MHz bandwidth available at 3 mm at the time.

---

[1] Four SMGs in our sample are members of close pairs (SMM J123711.98/ SMM J123712.12, and SMM J123711.86/SMM J123708.80), and in each case a single pointing was sufficient to observe both SMGs.

2.1.1 Deriving IR luminosities

As we have radio fluxes for our sources, we can derive the far-IR luminosity for our SMGs from the 1.4-GHz continuum, via the far-IR–radio correlation in Yun, Reddy & Condon (2001):

$$L_{FIR} = 4\pi D_L^2 \, (8.4 \times 10^{14}) \, S_{1.4} \, (1 + z)^{(\alpha - 1)}, \tag{1}$$

where D_L is the luminosity distance in metres, $S_{1.4}$ is the radio flux density at 1.4 GHz (in W m^{-2} Hz^{-1}) and α is the synchrotron slope used to K-correct the 1.4 GHz observations to the appropriate source redshift (α is taken here to be 0.8). This equation assumes $q_{FIR} = 2.34$. Some recent results from *Herschel* have suggested that a lower value ($q_{FIR} \sim 2.0$) may be appropriate for luminous SMGs (Ivison et al. 2010; Magnelli et al. 2012), which would lower our derived far-IR luminosities by a factor of ~ 2. However, no clear conclusion has yet been reached on this issue, so following Magnelli et al. (2012) we assume the (local) value of $q_{FIR} = 2.34$, and note the possibility of our far-IR luminosities being overestimated.

2.2 Data acquisition, reduction and analysis

The observations of SMGs described here were obtained in observing campaigns on the PdBI between 2002 and 2011, in good to excellent weather. The observations were undertaken with the lowest resolution 'D' configuration of the interferometer, in order to maximize the sensitivity, and used five of the six available antennas (giving a total of 10 baselines). The targets were observed in the 2- or 3-mm windows, depending upon the redshift of the source. The typical resulting resolution of our 3-mm maps is ~ 4 arcsec. Table 1 lists our observation log.

For data reduction, the IRAM GILDAS software was used. Data were carefully monitored throughout the tracks, and any bad or high phase noise visibilities were flagged. One or more bright quasars were typically used for passband calibration, and flux calibration was determined using observations of the main calibrators, 3C 454.3, 3C 345, 3C 273 and MWC 349. Phase and amplitude variations within each track were calibrated out by interleaving reference observations of nearby compact calibrators every twenty minutes (see Table 1). For the subsequent analysis, the routines CLIC and MAPPING were used, producing naturally weighted data cubes which were then outputted for analysis with our own IDL routines.

In a few cases, a line was detected close to the edge of the bandpass in the initial track. In these situations, the frequency setting was then adjusted to centre the line in the bandpass, and the source was re-observed. On average during the survey, a source was typically observed for 2–3 tracks (a total on-source integration time of 10–18 h). If no signal had been detected after this, the source was classed as a non-detection. Of the non-detections, subsequent observations (either in ^{12}CO, or from spectroscopy – either optical or near-/mid-IR) have shown that some of the originally targeted redshifts were incorrect and that the ^{12}CO lines likely fall outside of our band (Table 3) – we discard these sources. For eight of our non-detections, all the available evidence suggests that a ^{12}CO line should indeed lie within our band, and these we classify as 'true' non-detections. It should be noted here that the (non-detection) SMM J123629.13+621045.8 was followed up recently by Barger et al. (2012), with the those authors noting that the $z = 1.0130$ radio source was possibly misidentified as the source of the sum-mm emission. Here, we treat SMM J123629+621045 as a 'true' non-detection, but note the possibility of a redshift misidentification.

Table 4 lists the observed ^{12}CO properties of our SMGs. Fig. 1 shows example maps and spectra for two of the SMGs in our

Table 1. Observation log.

ID	ν_{obs} (GHz)	RMS$_{Band}$[a] (mJy)	RMS$_{Channel}$[b] (mJy)	On-source time (h)	Calibrator	Reference
SMM J021725.16−045934.7	139.5	0.15	0.80	5.3	3C 454.3	This work
SMM J021738.71−050339.7	151.9	0.15	0.80	4.1	3C 454.3	This work
SMM J021738.91−050528.4	130.6	0.15	0.80	5.1	3C 454.3	This work
SMM J030227.73+000653.3	95.73	0.15	0.80	13.1	0336−019	This work
SMM J044315.00+021002.0	150	0.17	0.7	–	–	Neri et al. (2003)
SMM J094304.08+470016.2	150	0.17	0.7	–	–	Neri et al. (2003)
SMM J105141.31+571952.0	104.12	0.12	0.68	19.3	0923+392	Engel et al. (2010)
SMM J105151.69+572636.0	87.92	0.05	0.51	8.7	0954+658	This work
SMM J105227.58+572512.4	99.94	0.09	0.84	7.1	0954+658	This work
SMM J105230.73+572209.5	96.02	0.12	0.65	21.9	1044+719	This work
SMM J105307.25+572430.9	91.33	0.05	0.38	16.4	0954+658	Bothwell et al. (2010)
SMM J123549.44+621536.8	107.95	0.12	0.65	11.4	1150+497	Tacconi et al. (2006)
SMM J123555.14+620901.7	80.46	0.19	1.0	11.0	1044+719	This work
SMM J123600.10+620253.5	115.49	0.42	2.2	9.4	1044+719	This work
SMM J123606.85+621047.2	98.65	0.14	0.78	18.0	1150+497	This work
SMM J123618.87+621007.5	107.72	0.06	0.57	13.0	1418+546	This work
SMM J123618.33+621550.5	153.73	0.09	0.64	18.6	1044+719	Bothwell et al. (2010)
SMM J123621.27+621708.4	154.19	0.15	1.0	7.3	0954+658	This work
SMM J123629.13+621045.8	114.52	0.34	1.8	6.1	1150+497	This work
SMM J123632.61+620800.1	115.48	0.54	2.9	20.1	1044+719	This work
SMM J123634.51+621241.0	103.71	0.13	0.79	15.1	1044+719	Engel et al. (2010)
SMM J123707.21+621408.1	99.08	0.16	0.85	9.6	1150+497	Tacconi et al. (2006)
SMM J123708.80+622202.0	159.86	0.21	1.0	17.5	1044+719	This work
SMM J123711.86+622212.6	159.86	0.21	1.0	17.5	1044+719	Casey et al. (2009)
SMM J123711.98+621325.7	115.41	0.33	1.8	12.3	1150+497	Bothwell et al. (2010)
SMM J123712.05+621212.3	88.37	0.08	0.55	17.8	1044+719	This work
SMM J123712.12+621322.2	115.41	0.33	1.8	12.3	1150+497	Bothwell et al. (2010)
SMM J131201.20+424208.8	99.60	0.39	0.70	10.2	1308+326	Greve et al. (2005)
SMM J131208.82+424129.1	90.62	0.10	0.60	18.8	1308+326	This work
SMM J131232.31+423949.5	103.90	0.39	2.1	0.9	1308+326	This work
SMM J163631.47+405546.9	105.53	0.16	0.83	9.7	3C 345	This work
SMM J163639.01+405635.9	92.65	0.28	1.5	5.5	3C 345	This work
SMM J163650.43+405734.5	102.17	0.07	0.38	40.4	3C 345	Neri et al. (2003)
SMM J163655.79+405909.5	95.52	0.15	1.1	7.0	3C 345	This work
SMM J163658.19+410523.8	100.11	0.12	0.73	14.9	3C 345	Greve et al. (2005)
SMM J163658.78+405728.1	105.24	0.20	1.0	8.3	3C 345	This work
SMM J163706.51+405313.8	102.51	0.13	0.76	13.9	3C 345	Greve et al. (2005)
SMM J221804.42+002154.4	98.32	0.13	0.63	24.8	2223−052	This work
SMM J221735.15+001537.2	84.44	0.10	0.52	16.5	2230+114	Greve et al. (2005)
SMM J221737.39+001025.1	95.52	0.15	0.78	14.4	2223−052	This work

[a]RMS noise averaged over the bandwidth of observation (= 1 GHz, except for the three 02-h SMGs which used the WideX correlator with a resultant bandwidth of 3.6 GHz).
[b]RMS noise per 20 MHz channel.

Table 2. List of sources with significant measured continuum.

ID	z	Continuum (predicted) [mJy]	Continuum (measured) [mJy]
SMM J021738−050339	2.037	0.35	0.36 ± 0.07
SMM J030227+000653	1.406	0.09	0.18 ± 0.05
SMM J123555+620901	1.864	0.07	0.16 ± 0.05
SMM J123618+621550	1.996	0.20	0.28 ± 0.02
SMM J123632+620800	1.993	0.19	0.51 ± 0.10
SMM J123634+621241	1.224	0.11	0.18 ± 0.03
SMM J163658+405728	1.192	0.14	0.27 ± 0.05
SMM J221804+002154	2.516	0.23	0.20 ± 0.03
SMM J163639+405635	1.488	0.09	0.46 ± 0.09

sample – the full sample of detections and non-detections are shown in the online supplementary material. In all but two cases, the SMGs were unresolved by our low-resolution observations, and a beam-averaged spectrum was extracted at the point of peak flux. In two cases (SMM J021738−050528 and SMM J221804+002154), emission was detected beyond the extent of the beam and flux was extracted in an aperture around the source.

Table 3. List of non-detection observations discarded due to a redshift measurement from the literature lying outside the band. (†SMG was later re-observed at the correct redshift.)

ID	z (targeted)	z (literature)	Redshift reference
SMM J105238+572435	3.045	2.99	Menéndez-Delmestre et al. (2009)
SMM J131232+423949†	2.321	2.332	Chapman et al. (2005)
SMM J123616+621513	2.55	2.578	Chapman et al. (2005)
SMM J123553+621337	2.098	2.17	Menéndez-Delmestre et al. (2009)
SMM J123635+621423	2.005	2.015	Swinbank et al. (2004)

Table 4. Median brightness temperature ratios for the SMGs in our sample. All errors estimated using bootstrap resampling.

Transition	Value
$r_{21/10}$	0.84 ± 0.13
$r_{32/10}$	0.52 ± 0.09
$r_{43/10}$	0.41 ± 0.07
$r_{54/10}$	0.32 ± 0.05
$r_{65/10}$	0.21 ± 0.04
$r_{76/10}$	0.18 ± 0.04

Of the 32 SMGs with detected ^{12}CO emission, it is important that we identify any 'marginal' cases, for which there is a chance that we have a false positive detection. For each of our detections, we identify any source with a peak flux >5 times the RMS map noise as a true detection. Sources with a peak flux <5σ were individually inspected for large spatial and velocity offsets (which we define as >4 arcsec from expected phase centre or >400 km s^{-1} from expected velocity zero-point, respectively), either of which result in the source being classified as a 'candidate' detection. We identify five such marginal cases; these are listed in Tables 4 and 5. In addition, we classify SMM J131208+4241 as a 'candidate' detection – despite being just ~1 arcsec from phase centre and ~300 km s^{-1} from the expected velocity zero-point, the source is only weakly detected (3.6σ), and as such we cannot say with confidence that it is a robust detection. These six candidate sources are hereafter identified separately in all figures.

Where we had detectable ^{12}CO emission, we determined the redshift (z) of the ^{12}CO emission by calculating the intensity-weighted peak redshift,

$$z_{\rm CO} = \frac{\sum (I(z)\,z)}{\sum I(z)}. \qquad (2)$$
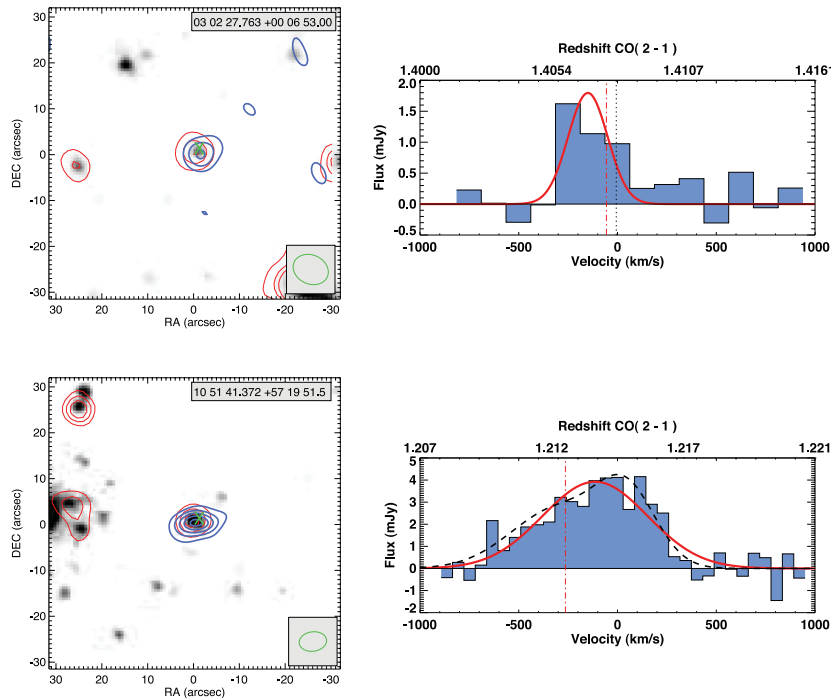
Figure 1. Example maps and ^{12}CO spectra for two of the SMGs in our sample (the full sample is shown in the online supplementary material). Top: SMM J030227.73. Bottom: SMM J105141.31. The maps show ^{12}CO (blue contours) and 24μm (red contours) overlaid on near-IR images made from the combined *Spitzer* IRAC images (3.6, 4.5, 5.8 and 8 μm). ^{12}CO contours start at 2σ significance, and are spaced in steps of 1σ (top) and 2σ (bottom). The cross shows the radio position, and the ellipse in the bottom right shows the synthesized PdBI beam. The spectra are taken at the point of maximum ^{12}CO intensity. The best-fitting single Gaussian profile is overlaid on each (and the best-fitting double Gaussian profile is shown for SMM J105141.31). The vertical dashed lines indicate redshift estimates from the literature: red shows redshifts derived from nebular recombination lines (Hα, or O[II]), black shows from UV emission lines (C05). Zero velocity corresponds to the central targeted frequency.

Table 5. Observational parameters of the programme SMGs.

ID	Transition	CO position (J2000)	z	I_{CO} [a] (Jy km s^{-1})	S/N (σ)	FWHM (km s^{-1})	$S_{850\,\mu m}$ [b] (mJy)	$S_{1.4\,GHz}$ [b] (μJy)
Detections								
SMM J021725−045934	(4–3)	02 17 25.16 −04 59 34.7	2.292	1.1 ± 0.19	4.7	850 ± 90	4.5 ± 1.9	57 ± 10
SMM J021738−050339	(4–3)	02 17 38.71 −05 03 39.7	2.037	3.2 ± 0.5	5.3	930 ± 70	4.4 ± 1.7	57 ± 10
SMM J021738−050528[c]	(4–3)	02 17 38.91 −05 05 28.4	2.541	1.9 ± 0.19	6.2	490 ± 60	7.1 ± 1.5	185 ± 12
SMM J030227+000653	(2–1)	03 02 27.66 +00 06 53.0	1.4060	0.40 ± 0.10	4.2	320 ± 40	4.4 ± 1.3	217 ± 9
SMM J044315+021002[d]	(3–2)	04 43 07.25 +02 10 23.3	2.5087	1.4 ± 0.2	7.0	350 ± 60	7.2	<60
SMM J094303+470016[e,f]	(4–3)	09 43 03.74 +47 00 15.0	3.3460	1.1 ± 0.1	11.0	420 ± 50	8.7	127
SMM J105141+571952	(2–1)	10 51 41.31 +57 19 52.0	1.2138	2.50 ± 0.19	10.7	625 ± 50	4.6 ± 1.6	295 ± 9
SMM J105151+572636	(2–1)	10 51 51.77 +57 26 35.3	1.5973	0.6 ± 0.3	6.2	700 ± 300	6.7 ± 1.7	134 ± 13
SMM J105227+572512	(3–2)	10 52 27.34 +57 25 17.6	2.4432	0.44 ± 0.11	5.0	310 ± 90	4.5 ± 1.3	39 ± 11
SMM J105307+572430	(2–1)	10 53 07.07 +57 24 31.9	1.5237	0.56 ± 0.08	6.9	320 ± 50	4.3 ± 2.2	56 ± 20
SMM J123549+621536	(3–2)	12 35 49.30 +62 15 36.8	2.2020	1.68 ± 0.17	9.3	590 ± 65	8.3 ± 2.5	74 ± 9
SMM J123555+620901	(2–1)	12 35 54.85 +62 08 54.7	1.8642	0.84 ± 0.3	4.3	380 ± 70	5.4 ± 1.9	212 ± 13
SMM J123606+621047	(3–2)	12 36 06.21 +62 10 24.9	2.5054	0.45 ± 0.15	4.3	350 ± 40	12 ± 4	74 ± 4
SMM J123618+621550	(4–3)	12 36 18.47 +62 15 51.0	1.9964	1.5 ± 0.2	8.6	1320 ± 120	7.3 ± 1.1	151 ± 11
SMM J123634+621241	(2–1)	12 36 34.57 +62 12 41.0	1.2245	1.5 ± 0.2	9.5	390 ± 40	4.3 ± 1.4	230 ± 14
SMM J123707+621408	(3–2)	12 37 07.28 +62 14 08.6	2.4870	1.0 ± 0.3	5.9	510 ± 70	4.7 ± 1.5	45 ± 8
SMM J123711+622212	(7–6)	12 37 11.86 +62 22 12.6	4.0510	1.6 ± 0.2	6.4	510 ± 150	20.3 ± 2.1[g]	73 ± 13[g]
SMM J123711+621325	(3–2)	12 37 11.19 +62 13 31.2	1.9951	1.9 ± 0.5	4.8	660 ± 140	4.2 ± 1.4	131 ± 8
SMM J123712+621322	(3–2)	12 37 12.12 +62 13 22.2	1.9964	1.2 ± 0.4	4.7	350 ± 100	4.2 ± 1.4	54 ± 8
SMM J131201+424208	(4–3)	13 12 01.20 +42 42 08.8	3.408	1.7 ± 0.3	5.7	530 ± 50	6.2 ± 1.2	49 ± 6
SMM J163650+405734	(3–2)	16 36 50.41 +40 57 34.4	2.3834	1.97 ± 0.14	8.1	910 ± 80	8.2 ± 1.7	221 ± 16
SMM J163658+410523	(3–2)	16 36 58.22 +41 05 23.4	2.4546	1.5 ± 0.2	5.0	660 ± 120	10.7 ± 2.0	92 ± 16
SMM J163658+405728	(2–1)	16 36 58.78 +40 57 27.6	1.1928	0.80 ± 0.18	6.3	220 ± 60	5.1 ± 1.4	74 ± 29
SMM J163706+405313	(3–2)	16 37 06.52 +40 53 15.6	2.3774	0.65 ± 0.15	4.4	430 ± 90	11.2 ± 2.9	74 ± 23
SMM J221804+002154[c]	(3–2)	22 18 04.47 +00 21 53.0	2.5166	1.3 ± 0.4	6.0	520 ± 100	9.0 ± 2.3	43 ± 10
SMM J221735+001537	(3–2)	22 17 35.10 +00 15 37.0	3.0963	0.7 ± 0.2	4.7	560 ± 110	4.9 ± 1.3	44 ± 13
Candidates								
SMM J123618+621007	(3–2)	12 36 19.37 +62 10 07.5	2.2030	0.28 ± 0.10	4.0	270 ± 90	6.7 ± 1.6[g]	100 ± 16[g]
SMM J123632+620800	(3–2)	12 36 33.04 +62 08 05.1	1.9938	1.8 ± 0.5	4.5	310 ± 110	5.5 ± 1.3	90 ± 9
SMM J131208+424129	(2–1)	13 12 08.75 +42 41 28.7	1.5432	0.67 ± 0.17	3.6	550 ± 40	4.9 ± 1.5	82 ± 5
SMM J131232+423949	(3–2)	13 12 32.13 +42 39 57.0	2.3298	2.0 ± 0.6	4.9	590 ± 100	4.7 ± 1.1	95 ± 4
SMM J163639+405635	(2–1)	16 36 39.32 +40 56 35.9	1.4883	0.40 ± 0.19	4.5	260 ± 80	5.1 ± 1.4	159 ± 27
SMM J221737+001025	(3–2)	22 17 37.59 +00 10 24.1	2.6149	0.29 ± 0.11	4.2	270 ± 50	6.1 ± 2.0	110 ± 14
Non-Detections[h,i]								
SMM J105230+572209	(3–2)	–	2.6011	< 0.23	–	–	11.0 ± 2.6	86 ± 15
SMM J123600+620253	(3–2)	–	1.9941	< 0.72	–	–	7.9 ± 2.0	131 ± 17
SMM J123621+621708	(4–3)	–	1.9902	< 0.41	–	–	7.8 ± 1.9	148 ± 11
SMM J123629+621045	(2–1)	–	1.0130	< 0.59	–	–	5.0 ± 1.3	81 ± 9
SMM J123708+622202[j]	(7–6)	–	4.0474	< 0.5	–	–	9.9 ± 2.3[k]	170 ± 13[k]
SMM J123712+621212	(3–2)	–	2.9131	< 0.20	–	–	8.0 ± 1.8	21 ± 4
SMM J163631+405546	(3–2)	–	2.2767	< 0.28	–	–	6.3 ± 1.9	159 ± 23
SMM J163655+405909	(3–2)	–	2.5900	< 0.40	–	–	8.7 ± 2.1[l]	200 ± 23[m]

[a] Errors here are Monte Carlo confidence intervals on the flux.
[b] From C05 (and references therein), unless otherwise stated.
[c] Extended source
[d] Lensed by a factor $\mu_L = 4.4$
[e] Actually two merging sources, H6+H7 – see Tacconi et al. (2006).
[f] Lensed by a factor $\mu_L = 1.2$
[g] Pope et al. (2006).
[h] CO upper limits derived as detailed in Section 4.3
[i] Redshifts for non-detections are quoted at the centre of the receiver bandwidth.
[j] Detected in ^{12}CO(4–3) by Daddi et al. (2009).
[k] From Chapman et al. (2001).
[l] Chapman et al. (2003).
[m] Biggs & Ivison (2006).

A linewidth can be estimated by measuring the full width at half-maximum (FWHM) of a Gaussian profile fit to the spectrum. However, if the line in question is non-Gaussian (for any number of reasons, such as showing an asymmetry, or being double-peaked), then a Gaussian profile will be a poor fit. To avoid this complication,

we use the intensity-weighted second moment (s_v) of the ^{12}CO spectrum as a non-parametric estimator of the linewidth:

$$s_v = \frac{\int (v - \bar{v})^2 \, I_v \, dv}{\int I_v \, dv}, \tag{3}$$

Table 6. Physical properties of the SMGs.

ID	L'_{CO}	$L'_{CO(1-0)}$ [a]	$\log_{10} M(H_2)$ [b]	$\log_{10} M_{dyn}$ (rotational)	$\log_{10} M_{dyn}$ (virial)	$\log_{10} M_\star$ [c]	$\log_{10} L_{FIR}$	AGN? [d]
	$(10^{10}$ K km s^{-1} pc$^2)$	$(10^{10}$ K km s^{-1} pc$^2)$	$(M_\odot)$	$(R_{kpc}$ $M_\odot)$	$(R_{kpc}$ $M_\odot)$	$(M_\odot)$	$(L_\odot)$	
Detections								
SMM J021725−045934	1.8 ± 0.6	4.4 ± 0.5	10.64 ± 0.03	10.66 ± 0.06	11.30 ± 0.06	–	12.64	–
SMM J021738−050339	4.2 ± 0.9	10.2 ± 3.0	11.01 ± 0.03	10.74 ± 0.04	11.38 ± 0.04	–	12.64	–
SMM J021738−050528	3.7 ± 1.1	8.9 ± 2.8	10.95 ± 0.03	10.18 ± 0.07	10.82 ± 0.07	–	12.64	–
SMM J030227+000653	1.0 ± 0.3	1.2 ± 1.4	10.09 ± 0.07	9.77 ± 0.06	10.41 ± 0.06	11.60	12.68	B
SMM J044315+021002 [e]	4.6 ± 1.4	11.4 ± 3.4	11.04 ± 0.13	9.89 ± 0.10	10.55 ± 0.10	–	12.47	–
SMM J094303+470016 [f]	3.9 ± 0.9	6.8 ± 1.6	10.82 ± 0.10	10.05 ± 0.07	10.70 ± 0.07	–	13.23	–
SMM J105141+571952	4.8 ± 0.4	5.8 ± 0.5	10.76 ± 0.03	10.39 ± 0.04	11.04 ± 0.04	–	12.64	–
SMM J105151+572636	2.0 ± 1.1	2.4 ± 1.4	10.4 ± 0.3	10.50 ± 0.4	11.14 ± 0.4	11.16	12.50	–
SMM J105227+572512	1.4 ± 0.3	2.7 ± 0.6	10.42 ± 0.12	9.78 ± 0.19	10.42 ± 0.19	11.24	12.79	–
SMM J105307+572430	1.7 ± 0.2	2.0 ± 0.3	10.30 ± 0.06	9.80 ± 0.08	10.45 ± 0.08	–	12.17	–
SMM J123549+621536	4.4 ± 0.4	8.4 ± 0.7	10.92 ± 0.05	10.35 ± 0.06	10.99 ± 0.06	11.20	12.68	–
SMM J123555+620901	3.6 ± 1.1	4.3 ± 1.5	10.64 ± 0.13	9.96 ± 0.11	10.60 ± 0.11	11.11	12.96	–
SMM J123606+621047	1.5 ± 0.5	2.8 ± 0.8	10.44 ± 0.14	9.89 ± 0.09	10.54 ± 0.09	10.30	12.80	C
SMM J123618+621550	1.8 ± 0.3	4.5 ± 0.6	10.64 ± 0.06	11.04 ± 0.05	11.69 ± 0.05	10.71	12.89	C, E
SMM J123634+621241	3.9 ± 0.3	3.5 ± 0.4	10.55 ± 0.04	9.98 ± 0.06	10.63 ± 0.06	10.82	12.56	–
SMM J123707+621408	2.9 ± 0.9	6.4 ± 1.5	10.80 ± 0.13	10.22 ± 0.07	10.86 ± 0.07	11.19	12.58	A
SMM J123711+622212	2.1 ± 1.0	11.6 ± 4.3	10.31 ± 0.17	10.22 ± 0.19	10.86 ± 0.19	11.36	13.27	–
SMM J123711+621325	4.2 ± 1.1	8.0 ± 1.7	10.90 ± 0.11	10.44 ± 0.13	11.08 ± 0.13	10.47	12.82	A
SMM J123712+621322	2.6 ± 0.8	5.0 ± 1.4	10.70 ± 0.14	9.89 ± 0.17	10.53 ± 0.17	11.19	12.43	–
SMM J131201+424208	5.9 ± 1.5	14.4 ± 3.8	11.15 ± 0.13	10.25 ± 0.05	10.89 ± 0.05	10.96	12.94	–
SMM J163650+405734	5.9 ± 0.4	11.2 ± 0.7	11.05 ± 0.03	10.72 ± 0.05	11.37 ± 0.05	10.99	13.23	B,C
SMM J163658+410523	4.7 ± 0.6	9.0 ± 1.0	10.95 ± 0.06	10.44 ± 0.11	11.09 ± 0.11	11.01	12.87	–
SMM J163658+405728	1.5 ± 0.3	1.9 ± 0.4	10.27 ± 0.10	9.47 ± 0.16	10.11 ± 0.16	10.89	12.04	–
SMM J163706+405313	1.9 ± 0.4	3.7 ± 0.7	10.56 ± 0.10	10.07 ± 0.17	10.71 ± 0.17	11.13	12.75	E
SMM J221804+002154	4.8 ± 0.7	9.4 ± 1.1	10.97 ± 0.10	10.23 ± 0.11	10.87 ± 0.11	10.79	12.50	–
SMM J221735+001537	3.3 ± 1.0	6.3 ± 1.6	10.80 ± 0.13	10.29 ± 0.12	10.94 ± 0.12	10.51	12.79	–
Candidates								
SMM J123618+621007	0.7 ± 0.3	1.4 ± 0.4	10.14 ± 0.17	9.65 ± 0.2	10.30 ± 0.2	–	12.71	–
SMM J123632+620800	3.8 ± 1.1	7.0 ± 1.8	10.84 ± 0.13	9.79 ± 0.18	10.43 ± 0.18	10.41	12.66	E
SMM J131208+424129	2.0 ± 0.5	2.5 ± 0.7	10.39 ± 0.12	10.28 ± 0.05	10.92 ± 0.05	10.86	12.36	–
SMM J131232+423949	5.7 ± 1.7	10.8 ± 2.9	11.03 ± 0.13	10.34 ± 0.10	10.99 ± 0.10	10.13	12.84	C,E
SMM J163639+405635	1.4 ± 0.5	1.7 ± 0.7	10.23 ± 0.11	9.62 ± 0.17	10.27 ± 0.17	10.59	12.60	–
SMM J221737+001025	1.0 ± 0.4	2.0 ± 0.7	10.29 ± 0.14	9.65 ± 0.11	10.30 ± 0.11	11.57	13.02	B,D
Sample median	3.3 ± 0.6	5.2 ± 1	10.71 ± 0.11	10.22 ± 0.10	10.86 ± 0.10	10.99	12.68	–
Non-Detections								
SMM J105230+572209	< 0.8	< 1.5	< 10.12	–	–	11.34	12.90	–
SMM J123600+620253	< 1.6	< 3.1	< 10.42	–	–	10.30	12.83	C,E
SMM J123621+621708	< 0.5	< 1.2	< 10.00	–	–	10.67	12.87	–
SMM J123629+621045	< 0.8	< 1.0	< 10.02	–	–	10.96	11.91	–
SMM J123708+622202	< 5.9	< 5.9	< 10.49	–	–	–	13.55	–
SMM J123712+621212	< 0.9	< 1.7	< 10.15	–	–	11.19	12.40	–
SMM J163631+405546	< 0.7	< 1.4	< 10.10	–	–	10.75	13.03	–
SMM J163655+405909	< 1.4	< 2.7	< 10.37	–	–	–	12.85	–

[a] Converted using an excitation model as detailed in Section 3.

[b] Assuming $\alpha = 1.0$ M$_\odot$ (K km s^{-1} pc$^2)^{-1}$

[c] From Hainline et al. (2011)

[d] Letters represent AGN activity diagnosed using the following estimators:

A = X-ray (Alexander et al. 2005)

B = Hα (Swinbank et al. 2004; Menéndez-Delmestre et al. 2009)

C = Power-law NIR component fractions (Hainline et al. 2011)

D = IRS spectral properties (Menéndez-Delmestre et al. 2009)

E = Colour selection (Ivison et al. 2004; Hainline et al. 2009)

[e] Lensed by a factor $\mu_L = 4.4$

[f] Lensed by a factor $\mu_L = 1.2$.

where $\bar{\nu}$ is the intensity-weighted frequency centroid of the line and I_ν is the flux as a function of frequency. In most cases, derived widths are similar (to within the errors) to those achieved with traditional Gaussian fitting. Variations occur only in low signal-to-

noise ratio (S/N) galaxies, where Gaussian fits struggle to achieve sensible results.

This non-parametric estimator does have the weakness of being sensitive to noise spikes in the spectrum – a large spike at the edge of

the receiver bandwidth can significantly broaden the effective width derived. To reduce this potential source of error, we used a Monte Carlo technique to generate multiple copies of each spectrum, with Gaussian noise added to each (as per the values given in Table 1). We took as our 'true' second moment the median value of the resultant distribution of intensity-weighted second moments.

The equivalent Gaussian FWHM of the line can then be calculated from the second moment, using the relation

$$\text{FWHM} = 2\sqrt{2\ln 2}\; s_\nu \;\simeq 2.35 s_\nu. \tag{4}$$

The flux density of each observed ^{12}CO line was found by velocity-integrating the ^{12}CO spectrum,

$$I_{CO} = \int_{z_{CO}-2s_\nu}^{z_{CO}+2s_\nu} I(\nu)\mathrm{d}\nu \tag{5}$$

(for a Gaussian emission line, this is equivalent to integrating the flux from -2σ to $+2\sigma$ around the centre). The ^{12}CO luminosities of the SMGs in our sample were then calculated using the standard relation given by Solomon & Vanden Bout (2005):

$$L'_{CO} = 3.25 \times 10^7\; S_{CO}\Delta\nu\; \nu_{obs}^{-2}\; D_L^2\; (1+z)^{-3}, \tag{6}$$

where $S\Delta\nu$ is the velocity-integrated line flux, L'_{CO} is the line luminosity in K km s^{-1} pc^2, ν_{obs} is the observed central frequency of the line and D_L is the luminosity distance in Mpc in our adopted cosmology.

We include in our fits the option for a positive uniform continuum, and detect significant continuum emission in nine sources (including two candidate sources, for which the continuum detection must be regarded as tentative). The measured continuum levels were then compared to extrapolations from 850-μm fluxes and far-IR luminosities, allowing for the evolution of the far-IR/radio correlation as described by Ivison et al. (2010), and adopting the 'greybody + powerlaw' fitting method described in Casey et al. 2012. In general, our sources show reasonable agreement between predicted and measured continuum values. There is a tendency for the measured continua to slightly exceed the predicted levels, which is to be expected given that the predicted levels are generally comparable to the noise levels of our spectra (with the result that continuum emission is only detected in sources with excess emission). Only one SMG (SMM J123632+6207) has a continuum level which exceeds the 'upper limit' on the continuum estimate (which is calculated allowing for uncertainty in the bolometric far-IR luminosities). SMM J123632 is a low S/N detection, and in the absence of other data we ascribe the apparent continuum excess to the low quality of the spectrum. Details for individual sources with significant continuum detections are given in Table 2.

For sources which are not detected in our ^{12}CO observations, we calculate 3σ line intensity limits based on the RMS channel noise:

$$I_{CO} < 3\,\text{RMS}_{channel}\;\sqrt{\Delta V_{CO}\,\mathrm{d}\nu}\;, \tag{7}$$

where RMS$_{channel}$ is the channel noise given in Table 1, ΔV_{CO} is the mean linewidth of the detected sample and dν is the bin size in km s^{-1}.

Importantly for the interpretation of the evolutionary properties of molecular gas, there is no apparent redshift bias in the detection probability: a Kolmogorov–Smirnov (K-S) analysis of the redshift distributions, sub-mm flux or 1.4-GHz continuum flux suggests that the non-detections are consistent with being a random selection drawn from the parent sample.

2.3 Comparing our sample to the wider SMG population

If we wish to use our sample to draw conclusions about the SMG population as a whole, it is important to investigate whether our ^{12}CO-detected sample is statistically representative of the wider (i.e. 850-μm bright, radio-detected) SMG population. For the purpose of comparison, we take as our 'representative' sample the large spectroscopic data base of SMGs presented by C05, which functions as an approximate parent sample to the sub-mm-selected, radio-detected and optical spectroscopy-confirmed SMGs presented in this work. Note that the selection of the C05 sample does imbue it with certain unavoidable biases – being sub-mm selected, it is biased towards colder sources (see Chapman et al. 2004; Casey et al. 2009a), and the radio-selection will tend to bias against higher redshift SMGs with weak radio emission. In addition, the necessity of a spectroscopic redshift confirmation will tend to bias the sample against sources which are UV-faint, or have weak emission or absorption features. Fig. 2 shows a comparison of three observable parameters (1.4-GHz continuum flux, 850-μm flux and R-band magnitude), as well as redshift distribution histograms, for the detected subset and the C05 parent sample.

Looking at the distribution of redshifts, our detected subset appears to be a representative sample of SMGs (with the aforementioned selection effects) at $z \sim 1$–3. We do not match the low-redshift coverage; however, low-redshift ($z < 1$) systems were not included in our programme, and as a result the lowest redshift SMG that was targeted in ^{12}CO is SMM J123629.13 at $z = 1.013$. Our observations also undersample the higher redshift range $z > 3$ when compared to C05.

As the remaining three panels show, the observable properties of our sample show no significant differences when compared to the parent, aside from what results from the redshift restrictions. The brightest R-band sources, for example, lie at $z < 1$ and do not appear in our sample. The 850-μm and 1.4-GHz flux distributions of sources appearing in our sample are also consistent with the equivalent distributions for the C05 sample sources, with no apparent bias towards more luminous systems. The mean 850-μm flux for our sample is 6.5 ± 0.6 mJy, compared to 5.9 ± 0.4 mJy for the C05 sample (cut to match the redshift coverage – i.e. $z > 1$ – of our sample); the respective radio flux densities are 114 ± 11 and 100 ± 12 μJy. K-S tests of the 850-μm and 1.4-GHz flux distributions suggest that our sample is statistically consistent with being drawn at random from that of C05. As a result, our sample of ^{12}CO-observed SMGs can be seen as representative of the brighter end of the population of $z \sim 1$–3 SMGs as a whole, at the era where the activity in this population peaks.

3 CO EXCITATION MODELLING

In order to derive the gas properties of our SMG sample, it is important to fully understand the gas excitation as shown by the ^{12}CO SLED. The excitation of a molecular gas reservoir is controlled by the physical conditions within the host galaxy: star-forming ULIRGs (and SMGs) are expected to have dense, excited gas that may be thermalized up to $J_{up} = 3$ or beyond (e.g. Weiss et al. 2007; Danielson et al. 2011), in contrast to the low-density, low-excitation gas which dominates the ^{12}CO emission of more quiescent galaxies (e.g. Crosthwaite & Turner 2007; Dannerbauer et al. 2009).

Even in luminous SMGs, however, the assumption that higher J_{up} transitions always trace fully thermalized gas is a poor one – as J_{up} increases, the observed gas becomes warmer and denser, and any underlying cold component can be missed (see Harris et al.
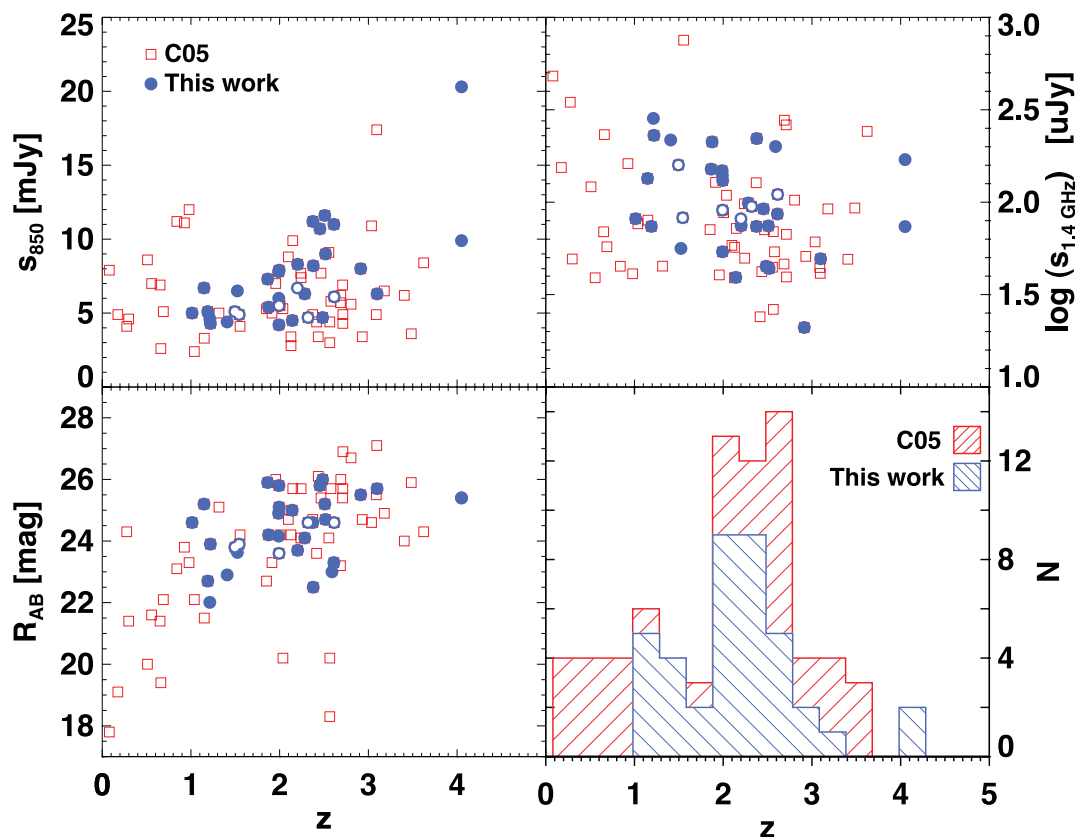
Figure 2. Plots comparing the observed properties of the ^{12}CO sample presented in this work, along with the 'parent' sample of C05. Here (and in plots hereafter), the open circles denote the SMGs we identify as 'candidate' detections, while the filled circles denote our secure detections. All four panels have redshift as the abscissa. The panels – top-left: 850-μm flux. Top-right: 1.4-GHz continuum flux. Bottom-left: *R*-band magnitude. Bottom-right: redshift distributions. Sources comprising our sample do not differ significantly from those in Chapman et al. (2005), over a similar redshift range.

2010; Ivison et al. 2010, 2011; Riechers et al. 2011). If we wish to fully investigate the physical conditions within our multiline survey (our data cover $J_{up} = 2$–7), it is important that we fully understand the typical SLED of SMGs from low- to high-J_{up} transitions. This SLED can then be used to derive a self-consistent excitation model.

Throughout this work, we use $r_{J, J-1/10}$ to denote the ratio of ^{12}CO luminosities[2] $L'_{CO}(J, J-1)/L'_{CO}(1-0) \equiv T_b(J, J-1)/T_b(1-0)$, where T_b is the equivalent Rayleigh–Jeans brightness temperature in excess of that of the cosmic microwave background.

In order to directly compare the SLEDs for multiple SMGs, it is important to remove the effect of the strong dependence of the ^{12}CO line luminosity on far-IR luminosity – without this step, the variation of L'_{CO} with L_{FIR} would introduce extraneous scatter (due to the gradient of the L'_{CO}–L_{FIR} relation). We therefore calculate a 'correction' factor, which will adjust the CO line luminosities to a common value of L_{FIR} (we use the mean of our sample, $= 6.0 \pm 0.6 \times 10^{12}$ L$_\odot$):

$$\Delta L'_{CO} = \frac{L_{FIR}}{\langle L_{FIR} \rangle}, \qquad (8)$$

which assumes a linear slope between L'_{CO} and L_{FIR} (see below). The correction factor to the CO fluxes, ΔS_{CO}, is then calculated from $\Delta L'_{CO}$, as per equation (6). After adjusting the line fluxes to a common L_{FIR}, SMGs with $L_{FIR} = \langle L_{FIR} \rangle$ will have their line fluxes

unchanged, and SMGs which are less (more) luminous will have their line fluxes proportionally increased (decreased).

The gradient of the L'_{CO}–L_{FIR} relation has been debated in recent years. Efforts at high redshift with small samples found a sub-linear slope: 0.62 ± 0.08, as given in Greve et al. (2005), for example. Recent analyses have suggested a somewhat steeper slope, with Genzel et al. (2010) and Daddi et al. (2010) reporting a near-linear slope for both SMGs and 'normal' SMGs. Below (Section 4.2), we discuss the slope of the L'_{CO}–L_{FIR} relation for the extrapolated ^{12}CO (1–0) luminosity, a physical quantity that has important implications for the SFE of our SMGs. For the purposes of removing L_{FIR}-induced scatter, we adopt a linear slope between L'_{CO} and L_{FIR}. We do note, however, that the resulting line luminosity ratios (quoted in Table 3) are relatively insensitive to the choice of slope – adopting a shallower slope has the effect of lowering the line luminosity ratios, but for a reasonable range of slopes (i.e. from 0.5–1.5) the variation in the resulting brightness temperature ratios due to the choice of slope is, at most, ~0.05.

The resulting ^{12}CO-line SLED for our sample of SMGs, adjusted to a common far-IR luminosity, is shown in Fig. 3. The fluxes have also been adjusted to a common source redshift of $z = 2.2$. In addition to the ^{12}CO line observations presented in this work, we have compiled all the observed transitions available in the literature for SMGs in our sample (compiled from Carilli et al. 2010; Riechers et al. 2010; Ivison et al. 2011). SMGs with multiple J_{up} transitions are highlighted in Fig. 3 and we also show the trend of the median ^{12}CO luminosity/flux as a function of J_{up}, which represents the SLED of 'typical' SMGs.

[2] In units of K km s^{-1} pc^2.
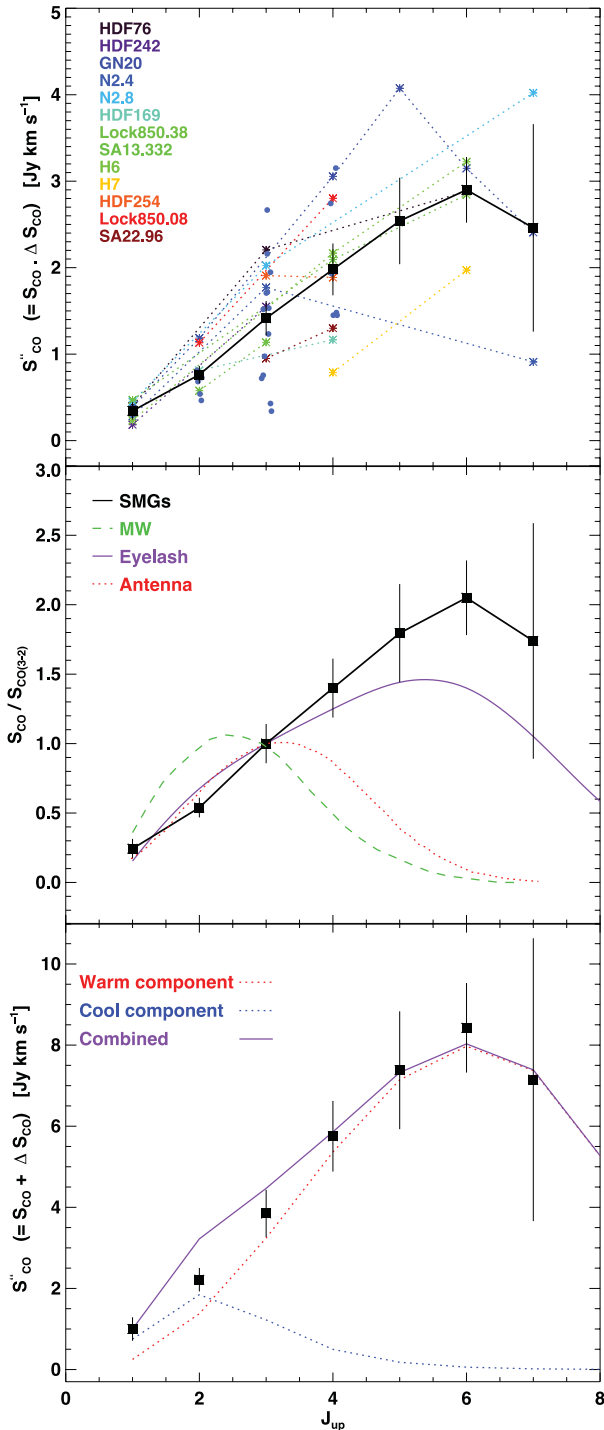
Figure 3. The ^{12}CO SLED for the SMGs in our sample. All SMGs have been normalized to the mean far-IR luminosity of the sample as detailed in the text, and fluxes have been adjusted to the median redshift of the sample ($z = 2.2$). Top: the ^{12}CO SLED for our SMGs, in (normalized) flux units. The SMGs in our sample with multiple J_{up} observations available in the literature are shown by connecting dotted lines. The colour coding is shown in the inset legend. SMGs with only a single observed transition are shown as blue circles. The median SLED of the sample, along with the bootstrapped error, is overlaid. Middle: the median SLED compared to other well-studied galaxies, normalized to the flux in the ^{12}CO (3–2) transition. Bottom: the median SLED, fitted with PDR models as discussed in the text. The median SLED shows a moderate excitation, similar to that of SMM J2135−0102 and is best fitted by a two-component model of the ISM.

As can be seen from the median line flux in the top panel of Fig. 3, the ^{12}CO SLED shows a moderate excitation. There is a monotonic increase in S_{CO} up to $J_{up} \sim 5$, with a flattening or turnover above this. This is similar to local starburst galaxies (see e.g. Weiss et al. 2007). The behaviour of the best-sampled SMG in our sample (SMM J123711.86 at $z = 4.04$ has five observed transitions) is not dissimilar to that of the median, showing an increase up to the $J_{up} = 5$ transition, and a turnover at higher excitations. We do caution, however, that the behaviour of the median SLED above the apparent turnover is poorly sampled, and dominated by low number statistics; hence, constraints on the higher excitation components must be taken as tentative.

The middle panel of Fig. 3 shows our derived ^{12}CO SLED, compared to three other well-studied systems, normalized to the ^{12}CO (3–2) flux. The moderate excitation found for our SMGs is certainly more excited than less-active, local galaxies. It is very similar, however, to the well-studied, strongly lensed SMG SMM J2135−0102 ('The Cosmic Eyelash'; Danielson et al. 2011), showing a similar peak and falloff towards higher J_{up}.

The bottom panel of Fig. 3 shows the results of fitting our SLED with the photon-dominated region (PDR) model of Meijerink, Spaans & Israel (2007). Single-component fits provided a poor fit to the data – hence, we are driven to a two-component model, consisting of separate 'warm' and 'cool' components, which provides a much better fit. The best fit is achieved with a combination is with 75 per cent of a cool component plus 25 per cent of the warm component. The cool component has a density $\log_{10}(n) = 2.0$ cm^{-3} and and a radiation field of $\log_{10}(G) = 1.5$ (where n is the hydrogen volume density density and G is the far-UV field strength in Habing units), and the warm component has a density $\log_{10}(n) = 5.5$ cm^{-3} and a radiation field of $\log_{10}(G) = 2.0$. Thus, the volume-averaged radiation field experienced by both components is between 30 and 100 times that of the Milky Way. Given the high SFRs for our SMG sample ($\sim$1000 times the Milky Way), these relatively modest radiation fields suggest their star formation must be spatially extended. Similarly, the characteristic densities we derive range between that expected for the ISM in typical SMGs and that in dense starburst systems (see fig. 4 in Danielson et al. 2011). As the bulk of the mass in these galaxies is in the cool component, we can use the best-fitting density for this component and assume that the gas is in a 1-kpc thick disc with a radius of $R \sim 3$ kpc (see Section 4.4) to predict a typical gas mass for an SMG of the order of $\sim 10^{11}$ M$_\odot$ comparable to the masses we estimate later in Section 4.4. However, we caution that acceptable model fits to the SLED span a significant range in parameters: the cool component can have a density of $2.0 < \log_{10}(n) < 3.0$ and a range of acceptable radiation fields of $1.0 < \log_{10}(G) < 2.5$, while the warm component parameters have ranges $4.5 < \log_{10}(n) < 6.5$ and $2.0 < \log_{10}(G) < 3.0$.

Using the SLED shown in Fig. 3, we calculate median brightness temperature ratios (equivalent to line luminosity ratios) which we use to convert our $J_{up} \geq 2$ observations into an equivalent ^{12}CO $J = 1$–0 flux. These are given in Table 4, and we use them throughout this work. These values agree well with values reported elsewhere in the literature (e.g. Ivison et al. 2011).

4 THE PHYSICAL PROPERTIES OF SMGS

In this section, we describe the models and methods used to derive physical parameters for our sample of SMGs – these are given in Table 5.
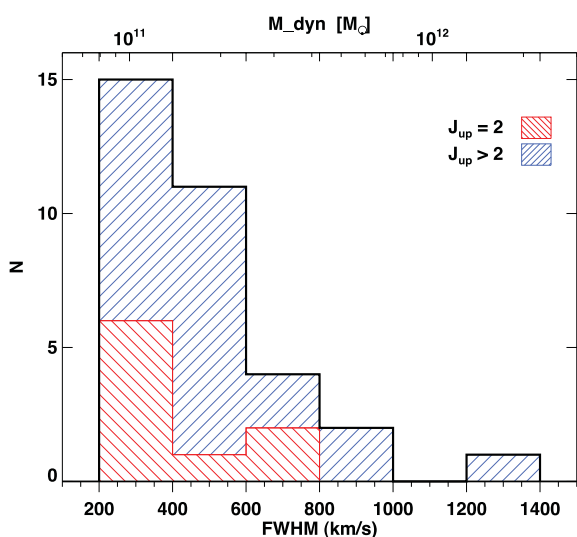
4.1 ^{12}CO kinematics

The ^{12}CO line emission from SMGs traces the kinematics of the potential well in which the molecular gas lies. Previous studies of this emission have uncovered very broad lines (Greve et al. 2005; Tacconi et al. 2006, 2008): Greve et al. (2005) found a mean FWHM linewidth of 780 km s^{-1} for their SMG sample, suggestive of deep gravitational potential wells.

The mean FWHM of our sample (which includes the Greve et al. 2005 SMGs) is 510 ± 80 km s^{-1}. This is somewhat lower than that found by Greve et al. (2005) and is most likely attributable to the bias towards IR-luminous sources in Greve et al. (2005) – the far-IR luminosities of their sample are higher than our sample, by a factor of ~ 2.5 [they quote $\langle L_{\rm FIR} \rangle = (15 \pm 7) \times 10^{12}$ L$_\odot$, whereas our sample has $\langle L_{\rm FIR} \rangle = (6.0 \pm 0.6) \times 10^{12}$ L$_\odot$]. As there is a strongly positive $L_{\rm FIR}-M_{\rm dyn}$ correlation (see Fig. 5), it is to be expected that the more IR-luminous SMGs presented in Greve et al. (2005) would have broader linewidths.

The distribution of FWHM values for our sample is shown in Fig. 4. The values derived from low $J_{\rm up}$ (i.e. $J = 2$–1) and higher $J_{\rm up}$ (i.e. $J_{\rm up} \geq 3$) lines have been highlighted separately. There is no significant difference between the two distributions – the mean values agree to within their 1σ errors (the $J = 2$–1 observations have a mean FWHM of 470 ± 80 km s^{-1}, compared to 550 ± 90 km s^{-1} for the $J_{\rm up} \geq 3$ sample), and a KS test gives a value of $P = 0.29$, suggesting that the data are consistent with the low-$J_{\rm up}$ FWHMs being selected at random from the distribution defined by the high-$J_{\rm up}$ sample.

Fig. 5 shows the FWHM of the observed emission line plotted against the (radio-derived) far-IR luminosity. Also shown in the plot are the 'sub-mm-faint radio galaxies' (Chapman et al. 2008; Casey et al. 2011), warmer dust counterparts of SMGs, and $z \sim 2$ optically selected SMGs (Tacconi et al. 2010), less-active SMGs at these epochs.

Of the three samples of galaxies shown in Fig. 5, our SMGs clearly have the largest linewidths. There is a significant overlap between the star-forming radio galaxies (SFRGs) and the SMGs,

suggesting that the 'hotter dust' ULIRGs are kinematically similar to SMGs (although the unknown inclinations add uncertainty to the conclusions drawn for any individual galaxy, by assuming that the inclinations are distributed randomly it is still possible to draw conclusions from the population as a whole – see Section 4.2 below for more discussion). The less-actively SFGs, however, have only a slight overlap with the SMGs, having typical linewidths <300 km s^{-1} – lower than all but the most narrow-line SMGs. Interestingly, the SFGs have far-IR luminosities a factor of several lower than even those narrow-line SMGs/SFRGs with compatible ^{12}CO FWHMs, suggesting that even SMGs which are kinematically comparable to optically selected galaxies have enhanced star formation. Dissecting the mechanisms driving this strong emission in the narrow-line SMG population requires high-resolution ^{12}CO imaging, in order to spatially resolve the kinematics.

Having measured ^{12}CO line luminosities and linewidths for our sample, we now turn to the correlation between these two observables, which respectively trace the mass of the gas reservoir and the dynamics of the potential well in which it lies. Fig. 5 shows the FWHM of the ^{12}CO emission line plotted against the derived ^{12}CO (1–0) luminosity for our sample of SMGs. Also shown in the plot are the ^{12}CO (1–0) observations for SMGs by Ivison et al. (2011). Included in the plot (but not included in any of the fits) are the $z \sim 0$ U/LIRGs from Downes & Solomon (1998). We fitted a power-law fit to the SMG sample, deriving a power-law index of 1.98 ± 0.07. The scatter around this power law is low – $\Delta L'_{\rm CO}/L'_{\rm CO} = 0.38$.
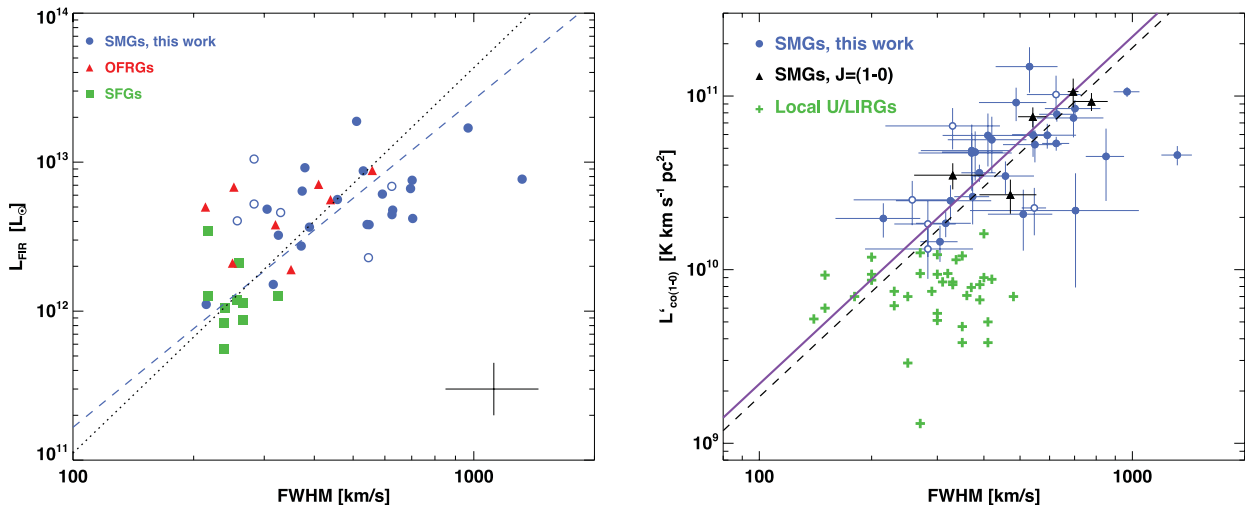
As $L'_{\rm CO}$ is sensitive to the total mass of molecular gas, while the FWHM is sensitive to both dynamical mass and any inclination effects, some dispersion around the relation would be expected. A population of thin, randomly orientated discs would introduce an inclination-based dispersion of ~ 50 per cent – the fact that our overall scatter is lower than this expected value strongly suggests that we are instead seeing gas in the form of thick discs (or turbulent ellipsoids), for which the line-of-sight velocity depends less strongly on inclination.

We also overlay a simple functional form for $L'_{\rm CO(1-0)}$:

$$L'_{\rm CO(1-0)} = \frac{C \, (V/2.35)^2 R}{1.36 \alpha G}, \tag{9}$$

where V is the FWHM ^{12}CO linewidth, 1.36α is the conversion factor from ^{12}CO line luminosity to gas mass (we adopt $\alpha = 1$; see Section 4.4 below), C is a constant parameterizing the kinematics of the galaxy (where we have taken $C = 2.1$ appropriate for a disc; see Erb et al. 2006), G is the gravitational constant and R is the radius of the ^{12}CO $J = 1$–0 emission region which, following Ivison et al. (2011) we have taken to be 7 kpc (see also Riechers et al. 2011). Section 4.2 below contains some discussion of the issue of ^{12}CO sizes.

This simple model provides a very good fit to the observed trend. Adopting $L'_{\rm CO(1-0)} \propto V^2$ is clearly a good match to luminous SMGs. The good correlation seen in high-redshift ULIRGs is in stark contrast to $z \sim 0$ U/LIRGs, which show very little correlation between V and $L'_{\rm CO(1-0)}$. We suggest that this is due to a combination of different geometry of the gas reservoirs; the thin nuclear gas discs and rings seen in local U/LIRGs mean that the lack of any inclination correction produces significant scatter in our plot, combined with a range in $f_{\rm gas}$ and a more significant stellar mass contribution to the dynamics of the potential well (there is little or no correlation between the stellar masses of the SMGs in our sample and their ^{12}CO linewidths).

Figure 4. Distribution of Gaussian-equivalent FWHMs for the source detected in ^{12}CO. FWHMs are derived from the intensity-weighted second moment, as described in Section 4.2. SMGs detected in 'high $J_{\rm up}$' ($J_{\rm up} \geq 3$) and 'low $J_{\rm up}$' ($J_{\rm up} = 2$) are plotted. As we discuss in the main text, there is no significant difference in the distribution between the two sub-samples.

Figure 5. Left-hand panel: L_{FIR} plotted against FWHM for the sample of ^{12}CO-detected SMGs. Also plotted are optically faint radio galaxies (OFRGs) from Chapman et al. (2008) and Casey et al. (2011), and $z \sim 2$ SFGs from Tacconi et al. (2010). The SFGs have IR luminosities several times lower than SMGs and star-forming radio galaxies (SFRGs), while displaying compatible linewidths to the low-linewidth end of the SMG distribution. The blue dashed line shows a power-law fit to the SMGs alone (index = 2.2 ± 0.2), and the black dotted line shows a fit to all three samples of galaxies (index = 2.6 ± 0.3). The SMGs have broader typical linewidths than other populations, and have enhanced far-IR luminosities compared to SFGs (even at comparable linewidths). Right-hand panel: $L'_{CO(1-0)}$ plotted against FWHM for the SMGs in this work. Also included are values for local U/LIRGs from Downes & Solomon (1998), and $J = 1-0$ observations of SMGs from the literature, but these are not included in the fits. The solid purple line shows the relation described in Section 4.1, while the dashed black line shows a simple fit to the points. The SMGs show a good correlation between $L'_{CO(1-0)}$ and FWHM.

This L'_{CO}–FWHM correlation either indicates a very uniform ratio of gas-to-stellar contribution to the dynamics of the region probed by the ^{12}CO emission, or that the gas mass dominates in this region (although that then requires the stellar mass to be significantly extended beyond the gas radius probed with our observations). There is little evidence for this; however, Swinbank et al. (2010) report *Hubble Space Telescope* NICMOS *H*-band radii of 2.8 ± 0.4 kpc for the SMGs, comparable to the extent of the high-J_{up} ^{12}CO emission (Bothwell et al. 2010; Engel et al. 2010).

4.1.1 Double-peaked sources

Looking in more detail at the spectra, some SMGs exhibit double-peaked ^{12}CO spectra – a potential indication of either the existence of kinematically distinct components within these systems, or a rotating disc-like component. Greve et al. (2005) found that four to six of their 12 ^{12}CO-detected SMGs displayed evidence of double-peaked CO lines (as did Tacconi et al. 2006, 2008 and Engel et al. 2010), and also suggested these tended to be the lower redshift systems. Our larger sample allows us to investigate these trends in more detail: we find that 7 of the 32 ^{12}CO-detected SMGs in the full sample are clearly double peaked, and a further 2 have spectra that are better-fitted by a double than a single Gaussian profile (measured by the reduced χ^2 of the fits). This is a lower fraction, 20–28 per cent, than previous findings. In addition, we do not find any evidence that the double-peaked sources lie at systematically lower redshift than the sample as a whole, in contrast to the suggestion of Greve et al. (2005).

We also note that we have seven examples of ^{12}CO sources which are spatially offset by $\sim$5–8 arcsec (= 40–60 kpc) from the initial spectroscopic targeted radio/Multiband Imaging Photometer (MIPS) source. These systems appear to indicate that there is both a high-redshift ULIRG and a gas-rich system in close proximity to each other, and we interpret these objects as further evidence for

a merger trigger in some SMGs. Combining these spatially offset systems and the double-peaked systems, we conclude that at least 14/32 SMGs (or 44 per cent) show some evidence for multiple components which appear indicative of a late-stage merger.

It must be noted that our observations can fail to detect kinematically distinct components in two situations. First, if the velocity separation between the components is too small they will appear as a single line. The typical peak separation of the double-peaked SMGs is $\sim$470 km s^{-1}, comparable to the mean linewidth of the sample ($\sim$500 km s^{-1}) – velocity separations much smaller than the linewidth will be blended. Secondly, the low spatial resolution of our maps cannot distinguish spatially separated components with similar line-of-sight velocities; our source SMM J094303+4700, for example, has been observed with higher resolution imaging, finding two distinct components (termed H6 and H7; Ledlow et al. 2002). This is also true of SMM J123707+6214 (Tacconi et al. 2008) and SMM J105307+5724 (Bothwell et al. 2010).

Thus, our 20–28 per cent fraction of double-peaked profiles should be interpreted as a lower limit to the true rate in SMGs.

Examining the physical properties of the double-peaked sources, we find that they do not seem to differ significantly from the population as a whole. The mean gas mass for double-peaked spectra is $(6.2 \pm 1.2) \times 10^{10}$ M$_\odot$, compared to $(5.3 \pm 1.0) \times 10^{10}$ M$_\odot$ for the complete sample. The mean far-IR luminosities for the respective classes differ by a comparable amount, with the double-peaked SMGs having a mean $L_{FIR} = (7.2 \pm 1.1) \times 10^{12}$ L$_\odot$, while the single-peaked galaxies have a mean $L_{FIR} = (6.0 \pm 0.6) \times 10^{12}$ L$_\odot$. That is, double-peaked sources have molecular gas reservoirs and far-IR luminosities approximately 20 per cent times greater than those with single peaks, but given the small numbers of sources examined these results are certainly not significant. If such offsets are confirmed with larger samples then this may be an indication that double-peaked sources represent mergers (in which there are several far-IR-bright components).

4.2 Dynamical masses

Our measurement of the kinematics of the ^{12}CO emission from SMGs allows us to estimate masses for the galaxies themselves from the width of the ^{12}CO line, with an assumption about the dynamical structure and extent of the system. For example, if the ^{12}CO emission arises in a virialized body of radius R, with one-dimensional velocity dispersion $\sigma = s_v$, then the dynamical mass is given by

$$M_{\mathrm{dyn}}\,(\mathrm{M}_\odot) = 1.56 \times 10^6\,\sigma^2\,R. \tag{10}$$

An alternative model for calculating dynamical masses is to assume that the line emission originates from a rotating disc. In this case, the dynamical mass is given by (i.e. Neri et al. 2003)

$$M_{\mathrm{dyn}}\sin^2 i\,(\mathrm{M}_\odot) = 4 \times 10^4\,V^2\,R, \tag{11}$$

where V is the FWHM velocity and i is the inclination of the disc. For the purpose of calculating dynamical masses using this method, we adopt a mean inclination angle, appropriate for a population of randomly orientated discs, of $\langle \sin i \rangle = \pi/4 \simeq 0.79$ (see appendix A of Law et al. 2009).

The choice of which estimator to use depends on the assumed form of the molecular ISM. If we assume that bright SMGs are predominantly major-merger events (as argued by Engel et al. 2010), then the virial estimator may be the correct choice. In contrast, the dynamics of the ^{12}CO emission from some SMGs (such as the lensed $z = 2.3$ SMG, SMM J2135−0102, which has been mapped at 100-pc resolution; Swinbank et al. 2010, 2011) have revealed that the molecular gas appears to lie in a rotating disc. However, the intrinsic luminosity of this galaxy is at the fainter end of our sample (Ivison et al. 2010). This is consistent with a mix of disc-like and virialized systems in the SMG population, with discs being more common at the lowest luminosities, while the brighter end of the SMG population has a higher frequency of merging systems. Of course, a rotating disc configuration does not preclude the conclusion that the galaxy is undergoing a merger, though it does suggest that any such merger is likely to be either in a very late or very early stage.

The final source of uncertainty in these calculations is the extent of the ^{12}CO emission. While the compact-configuration PdBI observations in our programme are well suited to a detection survey, they have the disadvantage of lacking the angular resolution necessary to resolve the emission in typical SMGs. Higher resolution observations from PdBI (typically in the higher J_{up} transitions) have suggested that the warm gas reservoirs in SMGs have measured radii of 2–3 kpc (Tacconi et al. 2008; Bothwell et al. 2010; Engel et al. 2010). Ivison et al. (2011), using ^{12}CO (1–0) observations of SMGs, suggested that the derived radius is also dependent on the transition observed; higher J_{up} lines preferentially trace denser and more centrally concentrated star-forming gas, yielding smaller radii, than the more extended reservoirs traced by lower J_{up} emission (which includes a more-extended component which may not be directly associated with vigorous star formation).

Examining all SMGs observed in high-resolution ^{12}CO (see the compilation presented by Engel et al. 2010), there seems to be something of a transition-based effect on the observed size of the ^{12}CO reservoirs in SMGs; the galaxies observed in ^{12}CO (4–3) emission have a mean radius of 2.1 ± 0.7 kpc, while those observed in ^{12}CO (3–2) have a mean radius of 3.1 ± 1.4 kpc (though these results should be taken as somewhat tentative, as sample sizes are small). The redshift ranges covered by the respective samples are similar, suggesting that this is not an evolutionary effect.

These high-J_{up} radii are smaller than the extents measured for ^{12}CO (1–0) emission; Ivison et al. (2011) found typical radii of ∼7 kpc for a sample of five SMGs, observed with the Jansky Very Large Array (JVLA). Those authors also find some evidence that the FWHM of the ^{12}CO (1–0) emission is ∼15 per cent broader than the higher J_{up} lines measured for the same SMGs, roughly consistent with the size variations.

With a likely variation in radius with transition, it could be argued that the correct radius to use for the dynamical calculation is the one appropriate for the transition used to derive the FWHM. However, one of the reasons for deriving the dynamical masses is to compare them to the 'total' gas and baryonic masses of these galaxies, we need to bear in mind that these 'total' measurements are effectively measured in an aperture equal to the size of the ^{12}CO (1–0) emission (as we are using galaxy-integrated $r_{J,\,J-1/10}$ values). The JVLA results suggesting a larger ^{12}CO radius are, however, as yet, based on small sample sizes.

To avoid introducing more uncertainty due to the choice of assumed size (which our low-resolution survey is not optimized to study), we explicitly retain the size dependence in our estimates of the dynamical masses. (For ease of comparison with other studies, we shall also quote the final values assuming both 'extreme' cases.)

The median dynamical mass derived for our sample depends on the choice of mass estimator. Adopting the 'virial' estimator given in equation (6), the median dynamical mass of the sample is $(7.1 \pm 1.0) \times 10^{10}\,R_{\mathrm{kpc}}\,\mathrm{M}_\odot$.[3] Removing the dependency on radius, this value corresponds to $(2.1 \pm 0.3) \times 10^{11}\,\mathrm{M}_\odot$ if we assume $R = 3$ kpc, and $(5.0 \pm 0.7) \times 10^{11}\,\mathrm{M}_\odot$ if we assume $R = 7$ kpc.

Alternately, adopting the 'rotational' (i.e. disc-like) estimator, given in equation (7), results in a median dynamical mass of $(1.6 \pm 0.3) \times 10^{10}\,R_{\mathrm{kpc}}\,\mathrm{M}_\odot$. Again removing the dependency on radius, this value corresponds to $(4.8 \pm 0.9) \times 10^{10}\,\mathrm{M}_\odot$ if we assume $R = 3$ kpc, and $(1.1 \pm 0.2) \times 10^{11}\,\mathrm{M}_\odot$ if we assume $R = 7$ kpc.

Each of these results are roughly in line with what might be expected from total halo masses; Hickox et al. (2012) found, using a clustering analysis, that SMGs typically lie within dark matter haloes of masses $M_{\mathrm{halo}} = 9 \times 10^{12}\,\mathrm{M}_\odot$.

These dynamical masses are also reasonably consistent with recent mass estimates for SMGs derived using other indicators. Swinbank et al. (2004, 2006) and Alaghband-Zadeh et al. (2012) used the kinematics of the spatially resolved Hα emission line to estimate the dynamical mass of a sample of bright SMGs, finding that a mass of $(5 \pm 3) \times 10^{11}\,\mathrm{M}_\odot$ represented the ensemble population well. The high dynamical masses found for SMGs are, in general, far greater than those found in other, less extreme samples of galaxies: galaxies comprising the UV-selected Spectroscopic Imaging survey in the Near-infrared with SINFONI (SINS) sample, for example have a typical dynamical mass of $8 \times 10^{10}\,\mathrm{M}_\odot$ (Förster Schreiber et al. 2006; Shapiro et al. 2009). Due to uncertain model parameters (size and choice of kinematic structure) inherent to a low-resolution study such as this, the range of possible dynamical masses is large. It is worth noting that a comparison to values derived from other studies (e.g. Swinbank et al. 2004, 2006) favours the upper end of our estimates, suggesting that systems which are both compact and disc-like perhaps do not comprise a significant proportion of the bright SMG population, and that extended and/or merging SMGs represent most of the SMGs in current studies. See Section 4.6 for more discussion of this issue.

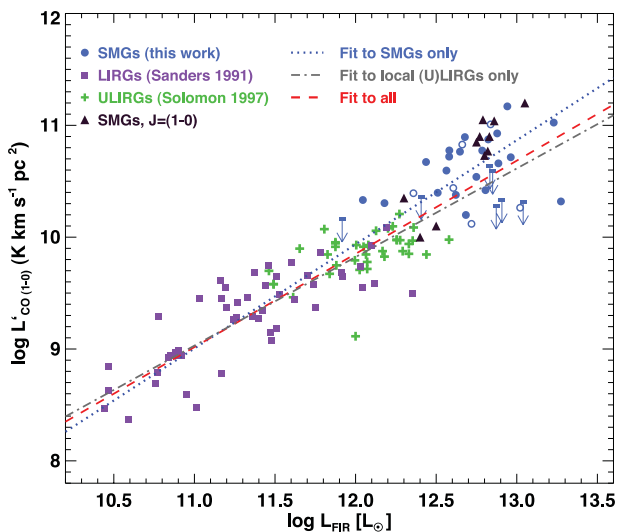[3] The error here is the statistical error resulting from uncertainty on the FWHM measures.

4.3 The L'_{CO}–L_{FIR} correlation

A useful quantity to measure for our sample of SMGs is the efficiency with which their molecular gas is being converted into stars. The SFE is sometimes defined as SFR/$M(H_2)$ – the inverse of the gas depletion time – but here we take the approach of parameterizing this as a ratio of observable quantities: L_{FIR} and $L'_{CO(1-0)}$.

There has been debate, in recent years, as to the value of the slope of the $L'_{CO(1-0)}$ – L_{FIR} relation. Whereas, earlier we discussed the difference in slopes between the various transitions observed (in order to derive the median SLED), here we present the relation between the derived ^{12}CO $J = 1$–0 luminosity and L_{FIR} – a relation which describes, in observable terms, the relationship between the luminosity due to star formation and the *total* gas content. (Section 2.1.1 contains a discussion of the uncertainties inherent to deriving IR luminosities for sources such as ours.)

In their study of 12 SMGs, Greve et al. (2005) found a slope of the relation between L_{FIR} and $L'_{CO(1-0)}$ of 0.62 ± 0.08 fit a combined sample of lower redshift LIRGs, ULIRGs and SMGs – identical to the slope derived for the local LIRGs/ULIRGs alone. The small number of galaxies in Greve et al. (2005), however, prevented a full investigation of the SFE slopes within the SMG population itself. Some recent authors, however, have found the slope to be closer to linear – Genzel et al. (2010) found that a slope of 0.87 ± 0.09 fits a combined sample of SMGs across a wide range of redshifts.

Fig. 6 shows the L'_{CO}–L_{FIR} relation for our sample of SMGs. Included in the plot are data points for local (U)LIRGs, as measured by Sanders, Scoville & Soifer (1991) and Solomon et al. (1997). We also show three power-law fits to the local (U)LIRGs alone, the SMGs alone and the combined sample. We find the SMGs to lie slightly above the best-fitting (sub-linear) line for local (U)LIRGs, necessitating a steeper slope. The power-law fit to the local (U)LIRGs alone has a slope of 0.79 ± 0.08, while the fit to the combined sample of SMGs and (U)LIRGs has a slope of 0.83 ± 0.09. It can also be seen that a fit to the SMG sample alone has an even steeper slope of 0.93 ± 0.14 – very close to linear – although, within the uncertainty, is consistent with the slope for the combined samples. These results are in good agreement with

most previous findings; the near-linear slopes (which agree well with those found by Genzel et al. 2010) would imply a roughly constant gas depletion time-scale across the entire range of far-IR luminosities shown here.

However, we caution that our analysis requires extrapolating from high-J_{up} ^{12}CO transitions to ^{12}CO (1–0). Ivison et al. (2010) have undertaken a similar analysis based solely on directly observed ^{12}CO (1–0) observations and homogeneously derived far-IR luminosities and conclude that the $L'_{CO(1-0)}$ – L_{FIR} relation has a slope substantially below unity. We therefore suggest that it is difficult to draw any strong conclusions from high-J_{up} observations about the gas depletion time-scales of the different populations or the form of the Kennicutt–Schmidt relation in these galaxies, as these are too uncertain without brightness temperature ratio measurements for individual sources.
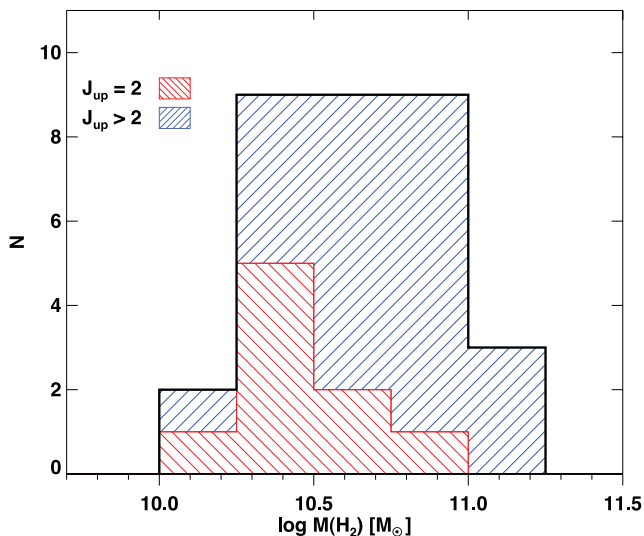
4.4 Molecular gas masses

Part of the power of observations of ^{12}CO emission from high-redshift galaxies is that they provide a tool to derive the mass of the reservoir of molecular gas in these systems. This is of critical importance because this reservoir is the raw material from which the future stellar mass in these systems is formed. Along with the existing stellar population, it therefore gives some indication of the potential stellar mass of the resulting galaxy at the end of the starburst phase (subject, of course, to the unknown contribution from in-falling and out-flowing material).

Estimating the mass of H_2 from the measured L'_{CO} requires two steps. First, luminosities originating from higher transitions ($J_{up} \geq 2$) must be transformed to an equivalent ^{12}CO $J = 1$–0 luminosity, using a brightness ratio. We have derived the necessary brightness ratios using our composite SLED as discussed in Section 3 above. Once an $L'_{CO(1-0)}$ has been determined, it must be converted into an H_2 mass by adopting a conversion factor α: $M(H_2) = \alpha L'_{CO}$, where α is in units of $M_\odot$ (K km s^{-1} pc^2)$^{-1}$ (when discussing α hereafter, we omit these units for the sake of brevity). This can then be converted to a total gas mass, including He, $M_{gas} = 1.36 M(H_2)$.

There is a large body of work, both observational and theoretical, dedicated to determining the value – and ascertaining the metallicity or environmental dependence – of α (e.g. Young & Scoville 1991; Solomon & Vanden Bout 2005; Liszt, Pety & Lucas 2010; Bolatto et al. 2011; Genzel et al. 2012; Narayanan et al. 2011; Papadopoulos et al. 2012). While secular discs such as the Milky Way have a relatively 'high' value of $\alpha \sim 3$–5, using this value for the gas in nuclear discs/rings within merging systems and starbursts at $z \sim 0$ leads to the molecular gas mass sometimes exceeding their dynamical masses. As such, a lower value – motivated by a radiative transfer model of the ^{12}CO kinematics – is typically used for the intense nuclear starbursts in the most IR-luminous local systems: $\alpha \sim 0.8$, with a range of 0.3–1.3 (Downes & Solomon 1998). However, some recent results have suggested that this value might, in fact, *underestimate* the true value in high-redshift SMGs. Bothwell et al. (2010) found that applying the canonical ULIRG value to two $z \sim 2$ SMGs resulted in gas fractions of <10 per cent, which appears incongruous given their extreme SFRs. Similarly, a dynamical analysis has been undertaken on the high-redshift SMG, SMM J2135−0102, by Swinbank et al. (2011) yielding a higher value, $\alpha \sim 2$ [supported by Large Velocity Gradient (LVG) modelling; Danielson et al. 2011].

Here we adopt a value of $\alpha = 1.0$, and caution that all gas masses derived are dependent on this uncertain parameter. Using this value, the resulting mean H_2 mass of our sample SMGs (including limits

Figure 6. The SFE, L'_{CO} versus L_{FIR}. Included in the plot are two samples of local ULIRGs, and the $J = (1$–0) SMG observations of Ivison et al. (2011). Best-fitting slopes to the SMGs alone, the local ULIRGs alone and all three combined samples are overplotted. They have slopes of 0.93 ± 0.14, 0.79 ± 0.08 and 0.83 ± 0.09, respectively.

Figure 7. Distribution of H_2 gas masses for the full sample. To calculate H_2 masses, a $^{12}CO/H_2$ conversion factor of $\alpha = 1.0$ has been assumed as detailed in Section 4.4. We identify both 'high J_{up}' and 'low J_{up}' derived masses; the offset between these most probably arises due to a redshift bias, whereas the 'low-J_{up}' sources are smaller galaxies lying at a lower mean redshift.

from the non-detections) is $(5.3 \pm 1.0) \times 10^{10}$ M$_\odot$. This is comparable to the findings of Greve et al. (2005), once the conversion factor and excitation model (detailed in Section 3) is accounted for; adjusted for our model values, the SMGs presented in that work have a mean gas mass of $(6.5 \pm 2.2) \times 10^{10}$ M$_\odot$.

The distribution of H_2 masses for our sample is shown in Fig. 7. As previously, we have differentiated in the distribution between low-J_{up} ($J_{up} = 2$) and higher J_{up} ($J_{up} \geq 3$) lines. There is a notable tendency for the low-J_{up} lines to result in lower gas masses than the higher J_{up} subsample. The mean gas mass for the $J_{up} = 2$ subsample is $(3.2 \pm 2.1) \times 10^{10}$ M$_\odot$, compared to a mean gas mass of $(6.2 \pm 0.2) \times 10^{10}$ M$_\odot$ for the SMGs observed in higher J_{up} transitions. This factor of ~ 2 difference is substantially more than could be attributed to random errors in the adopted brightness model, and it likely a result of the low-J_{up} observed SMGs lying at a lower mean redshift (and therefore having a lower mean far-IR luminosity; see Fig. 4, where a similar effect is seen in the distribution of linewidths). Splitting our SMG sample into low-redshift ($z < 2$) and high-redshift ($z > 2$) subsamples, we find H_2 masses of $(4.1 \pm 1.0) \times 10^{10}$ and $(6.1 \pm 0.2) \times 10^{10}$ M$_\odot$, respectively.

The gas masses determined for our sample of SMGs are roughly comparable to those derived for other high-redshift SMGs (though differences in $^{12}CO/H_2$ conversion factor make comparisons difficult). Tacconi et al. (2010) find mean molecular hydrogen masses of $(7.9 \pm 2.9) \times 10^{10}$ and $(1.3 \pm 0.7) \times 10^{11}$ M$_\odot$, respectively for their low-redshift ($z \sim 1.2$) and high-redshift ($z \sim 2.3$) samples of 'main-sequence' SMGs (selected from the AEGIS and BX/BM surveys). These are similar to our estimates, but we note that the two samples were calculated with very different values of α – Tacconi et al. (2010) adopt a value of $\alpha = 3.2$, more appropriate for secular disc galaxies and a factor of 3 higher than the $\alpha = 1$ we use for our SMGs.

4.5 The evolution of the gas fraction

If it is true that all star formation follows a universal scaling law dependent solely on the available gas, then the peak in cosmic star

formation activity – and subsequent decline – is simply a reflection of the availability of molecular gas within galaxies. Recent results have strengthened the expectation that normal, SMGs at high redshift are substantially more gas rich than their $z \sim 0$ counterparts, by perhaps a factor of 3–10 (Daddi et al. 2010; Tacconi et al. 2010; Geach et al. 2011). As pointed out by Davé, Finlator & Oppenheimer (2011), the drop in gas fraction between high redshift and the present day could be a straightforward result of the gas supply rate dropping faster than the gas consumption rate. Conversely, a gas fraction which rises with time represents a rapid accretion rate which swamps the consumption rate, leading to the accumulation of large gas reservoirs (thought to occur at $z \gtrsim 4$; Davé et al. 2011; Papovich et al. 2011). The implication of this, of course, is that the enhanced SFRs seen in these normal SMGs at $z > 1$ do not necessarily represent a 'superefficient' mode of star formation, but could instead simply reflect the larger gas reservoirs available in the early Universe (potentially driven by correspondingly larger accretion rates from their surroundings).

The gas content of galaxies is controlled by three main processes; gas accretion via inflow from the intergalactic medium, gas consumption due to driven by star formation and outflows due to both AGN and star formation. We can define the baryonic gas fraction, $f_{gas} = M_{gas}/(M_{gas} + M_\star)$, where M_{gas} includes helium.[4] The gas fraction represents the product of these opposing factors, and the evolution of f_{gas} therefore encodes important information about their relative strength over time.

Fig. 8 shows the baryonic gas fraction for our sample of SMGs. To extend the redshift range of the plot we include four SMGs at high redshift ($z > 4$), as recently presented by Schinnerer et al. (2008), Daddi et al. (2009), Coppin et al. (2010) and Riechers et al. (2010), in addition to GN20 in our sample at $z = 4.05$. We see a substantial variation in f_{gas} across the population, with values ranging from 0.1 to 0.9. However, overall we find the SMGs to be very gas rich, as expected, with a median $f_{gas} = 0.43 \pm 0.05$. The evolution of the mean SMG f_{gas} is overplotted in Fig. 8. We include in this plot the mean value for SMGs in the local Universe (Bothwell et al. 2009) as well measurements of UV-selected SMGs at $z \gtrsim 1$ from Tacconi et al. (2010) and Daddi et al. (2010), and mid-IR-selected $z \sim 0.4$ LIRGs from Geach et al. (2011). Note that these samples of galaxies use differing values of α appropriate for their respective types; Tacconi et al. (2010) adopt $\alpha = 3.2$, Daddi et al. (2010) use $\alpha = 3.6$, while Geach et al. (2011) and Bothwell et al. (2009) use a local 'Galactic' value of 4.6.

It is notable that while SMGs are clearly highly gas-rich systems: at every epoch in our sample molecular gas represents 40–60 per cent of their total baryonic content, they do *not* appear to be more gas rich than 'normal' SMGs at comparable redshifts, despite being selected to be a strongly star-forming population. Indeed, although they have comparable baryonic gas fractions, the Tacconi et al. (2010) galaxies have mean SFRs of 100 M$_\odot$ yr^{-1} at $z \sim 1.2$, and 150 M$_\odot$ yr^{-1} at $z \sim 2.3$, lower than the SFRs of our SMG sample at the same redshifts (Table 5) by factors of ~ 4 and ~ 8, respectively. The comparable gas fractions indicate that the SMGs are no less evolved – in terms of their gas properties – than less-active galaxies at similar epochs.

---

[4] Here, stellar masses have been taken from Hainline et al. (2011), who fit stellar population synthesis models to (observed-frame) optical through mid-IR SEDs. The typical stellar mass uncertainty, excluding IMF systematics, is 10–15 per cent.
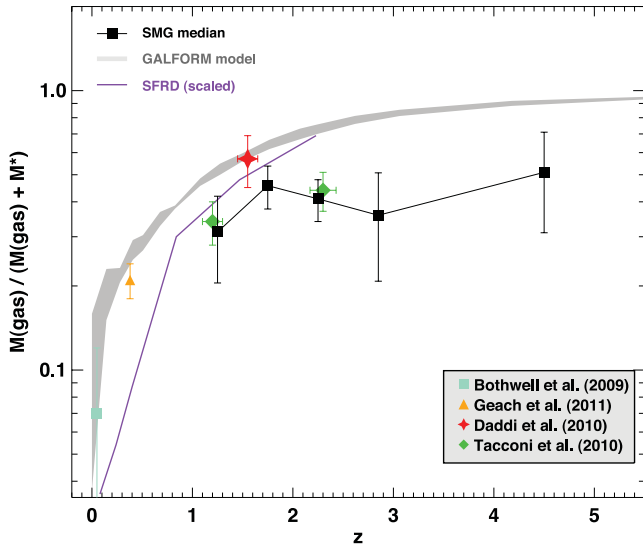
Figure 8. The redshift evolution of the baryonic gas fraction. The evolution of the mean baryonic gas fraction for our SMG sample, calculated in bins of width $\Delta z = 0.5$, is overlaid (due to the paucity of high-redshift SMGs, the final bin is the mean for all $z > 3$ SMGs). We also plot SMGs from the literature as follows: at $z \sim 0$ (Bothwell, Kennicutt & Lee 2009); $z \sim 0.4$ (Geach et al. 2011); $z \sim 1.5$ (Daddi et al. 2010); $z \sim 1.2$ and $z \sim 2.3$ (Tacconi et al. 2010). We also plot, as a grey shaded area, the GALFORM predictions for the evolution of the baryonic gas fraction for LIRGs ($L_{\mathrm{FIR}} > 10^{11}$ L$_\odot$) with halo masses between 10^{12} and 10^{13} M$_\odot$ (Lagos et al. 2011). There appears to be very little evolution in the mean SMG gas fraction over a wide interval of cosmic time. Furthermore, our SMGs exhibit similar gas fractions to lower luminosity, optically selected populations at comparable redshifts. A schematic representation of the evolution of the SFRD (Sobral et al. 2013) is overlaid – it can be seen that the behaviour of the SFRD broadly follows the global evolution of the gas fractions.

It is also interesting to note the redshift evolution of the baryonic gas fraction. The median gas fraction of the sample remains approximately constant across the redshift range of our sample, down to $z \sim 1.5$. There is a steep decrease in the mean gas fraction of galaxies below $z \sim 1$, however, with median gas fractions dropping to $\sim$20 per cent by $z \sim 0.4$ (Geach et al. 2011), and $<$10 per cent for typical SMGs in the local Universe (Bothwell et al. 2009). This drop below $z \sim 1$ coincides with both the observationally observed drop in global star formation rate density (SFRD; e.g. Hopkins & Beacom 2006; Sobral et al. 2011 – shown in Fig. 8), and the theoretically predicted fall in specific accretion rates (Krumholz & Dekel 2012). It seems that with globally falling accretion rates below $z \sim 2$, the mean mass of the gas reservoirs available to fuel starbursts decreases.

In order to compare to simulations, we also include in Fig. 8 the predictions from the semi-analytic galaxy formation model GALFORM (Lagos et al. 2011; see also Swinbank et al. 2008). For this analysis, we applied an 'LIRG' selection criteria, so that only galaxies with $L_{\mathrm{FIR}} > 10^{11}$ L$_\odot$ were considered. In order to have a reasonable comparison to the SMG population, we also only considered galaxies inhabiting the most massive haloes, with masses of 10^{12}–10^{13} M$_\odot$ (Hickox et al. 2012). It is clear that the real SMGs are somewhat gas deficient compared to those in the semi-analytical model, which predicts very high median gas fractions of $>$70 per cent above $z \sim 2$. Swinbank et al. (2008) drew a similar conclusion from their comparison of the GALFORM predictions for SMGs with observations that the model had too many of the baryons in $z \sim 2$ sub-mm-selected ULIRGs in the form of gas, compared to their

mass of stars. Thus, it appears that the model needs to increase the efficiency of star formation in massive galaxies at high redshifts to match the observations.

Other cosmological models fare somewhat better when compared to our observational data. The cosmological hydrodynamic simulations of Davé et al. (2011) predict smaller gas fractions for massive galaxies at high redshift – typically $\sim$30 per cent for a galaxy with a stellar mass of 10^{11} M$_\odot$ at $z \sim 2$ closer to the current observations (the precise figure depends on input parameters, such as the choice of wind model). However, a major weakness of this comparison is that these model galaxies do not have a 'high-SFR' criterion applied to them (to attempt to approximate SMGs) and so the relevance of this model comparison to the SMG population is not clear.

4.6 A comparison of mass measurements

As explained above, there are several properties of the SMG population which a detection survey such as ours is not ideally suited to study. These include the size of the ^{12}CO reservoir, as well as the kinematic mode dominating the gas dynamics (which we present as either rotational or virialized). These quantities can be studied in tandem, however, in order to try to explore the range of physically motivated parameters that describe the SMG population. As an example, it is unlikely that the SMG population as a whole is both rotation dominated and compact,[5] as the total dynamical masses derived under these assumptions are typically lower than our adopted stellar masses (which provide only one component of the total gravitational potential).

It is possible to explore the range of parameters which result in physically plausible outcomes. The dynamical masses (derived above) and the total baryonic masses (our gas masses plus stellar masses derived by Hainline et al. 2011) of our SMGs effectively function as independent measurements of the total mass in the central regions of the galaxies (where the baryons are expected to dominate the kinematics; see Section 4.1). As a test of what constitutes a 'physically plausible' set of parameters, we allow α to vary, calculating the value of α required in order to force agreement between the two independent measurements of the total mass. In other words, we assume

$$\frac{1.36\alpha L'_{\mathrm{CO}} + M_*}{M_{\mathrm{dyn}}} = 1, \qquad (12)$$

(where the factor 1.36 is to account for interstellar helium). Just as a combination of compact (3 kpc) sizes and rotational kinematics results in a mean $M_\star > M_{\mathrm{dyn}}$ (in our formalism above, implying a negative value of α), a combination of extended (7 kpc) sizes and virialized kinematics causes a similarly unphysical outcome. The dynamical masses derived in this circumstance are large enough to require a value of $\alpha = 4.9 \pm 0.8$ – greater even than the value adopted for secular discs at $z \sim 0$, and likely to be inappropriate for highly luminous starbursts, such as SMGs (see Solomon & Vanden Bout 2005). Alternately, these large dynamical masses imply a dominant dark matter component to the kinematics of the SMG, something which is again unlikely (see Section 4.1).

The two combinations that result in a physically motivated value of α, compatible (to within a factor of 2) to values adopted typically adopted for ULIRGs/SMGs, are (1) compact sizes and virialized kinematics and (2) extended sizes and rotational kinematics. Fig. 9

---

[5] Which, as above, we take to mean a fiducial radius of 3 kpc; similarly, in this discussion we take 'extended' to mean a fiducial radius of 7 kpc.
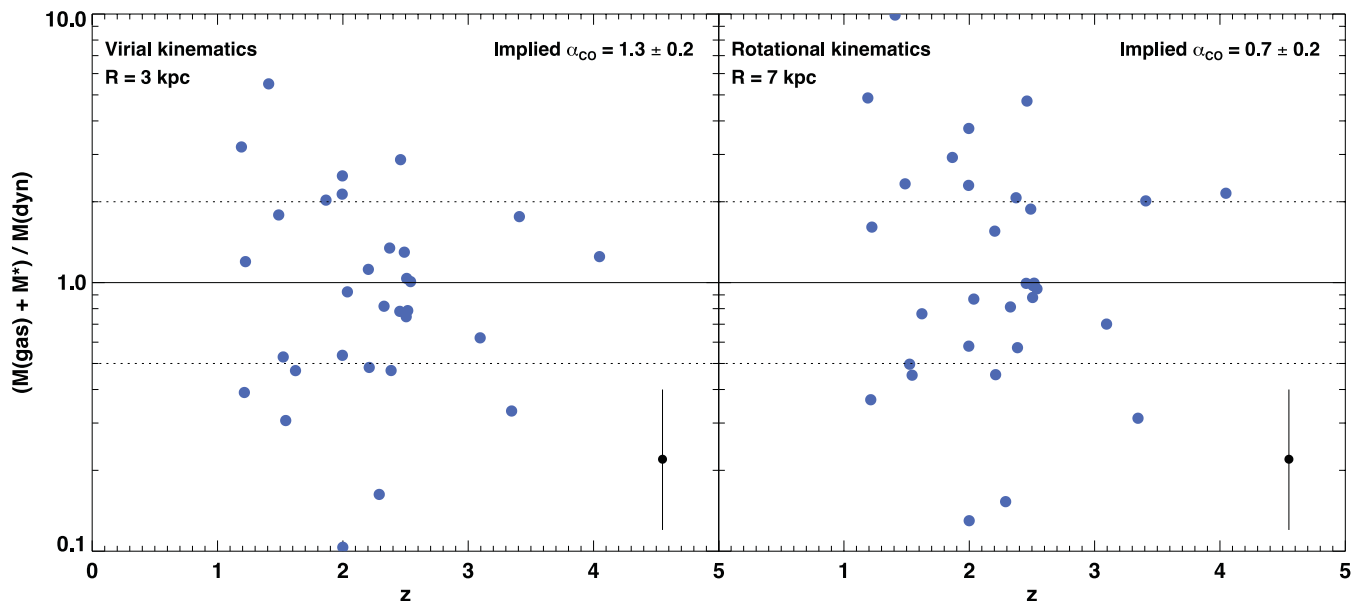
Figure 9. The ratio of total baryonic mass (the sum of the gas plus stellar masses) to dynamical mass, plotted against redshift, for both kinematical models of SMGs (rotational kinematics shown in the right-hand panel, and virialized kinematics shown in the left-hand panel). As the central regions of the SMGs – traced by the molecular gas – are expected to be baryon dominated, we determine the value of the ^{12}CO/H$_2$ conversion factor (α) necessary to result of this ratio of unity (the values are reported in the respective panels). This figure also illustrates the scatter of the SMG population around this median ratio, which is larger than the 1σ error (shown in the bottom-right), and may, in part, be driven by our assumption of a single model to describe to all SMGs. A median ratio of unity is indicated with a solid line, and dotted lines indicate a factor of 2 variation.

shows the ratio of the total baryonic mass to dynamical mass for both of these models of our ^{12}CO-detected sample, plotted against redshift.

There is a large scatter in each plot, indicative of the large uncertainties on each parameter (including the population averaged value of $\sin(i)$ adopted in the rotational estimator). However, the scatter in the population is, in each case, larger than the expected 1σ error (indicated in the bottom-right), implying that there is a significant variation in the value of our derived mass ratio across the population. Given that the innate mass ratio is likely to be very close to unity (modulo a small dark matter contribution), this additional scatter, beyond the formal error, is likely a result of the globally chosen parameters applying poorly to some individual SMGs – an incorrect value of α, for example, or an incorrect ^{12}CO radius. This suggests that the models being discussed here almost certainly do not apply universally, across the entire SMG population – even in an average sense.

As discussed above, it seems likely that the SMG population is a heterogeneous mix of merger-like and disc-like galaxies, with the relative contribution of these to the total population varying as a function of luminosity. Considered within this framework, it could be argued that the SMG population contains both systems in which the gas reservoir is 'compact and virialized', and 'extended and rotation dominated', with the former corresponding to the luminous 'merger' systems, and the latter representing the more 'disc-like' systems (such as the 'Eyelash', SMM J2135−0102). Solidifying this picture, however, will require higher resolution measurements of ^{12}CO in a large number of SMGs, capable of resolving the kinematic structure and the extent of the ^{12}CO reservoir. Using such measurements, it could also be possible to use this technique to place dynamical constraints on the value of the ^{12}CO/H$_2$ factor α for the SMG population.

5 THE EVOLUTION OF SMBHS IN SMGS

The characterization of SMBHs in high-redshift SMG hosts has the potential to shed light on the co-evolution of SMBHs and spheroids, an important facet of galaxy formation studies. It is well known that there exists a correlation between the mass of an SMHB (M_{BH}) and the velocity dispersion (σ) of its host spheroid: $M_{BH}-\sigma$ (Magorrian et al. 1998), implying well-regulated feedback mechanisms in place which couple the two components. Indeed, the correlation is so good that the scatter is no more than would be expected from pure measurement error alone (Ferrarese & Merritt 2000). This tight correlation suggests a symbiosis between galaxy formation and the formation of the central SMBHs, feedback from which is thought to play an integral part in the evolution of the most massive galaxies (e.g. Benson et al. 2003).

5.1 AGN-dominated SMGs

As reported by Alexander et al. (2005a), the high AGN fraction seen in the SMG population indicates relatively continuous BH growth occurring throughout the intense star formation phase. This is in line with theoretical models of ULIRGs and SMGs (i.e. Narayanan et al. 2010): major mergers efficiently transport gas into the dense central regions, which – as well as fuelling a nuclear starburst – can efficiently 'feed' a BH.

While observational studies of SMGs have generally concluded that their prodigious bolometric luminosities are powered star formation activity (e.g. Frayer et al. 1998, 1999; Alexander et al. 2005b; but see Hill & Shanks 2011), many studies have found that a significant minority of SMGs do host a luminous AGN (Alexander et al. 2005a, 2008; Lutz et al. 2010; Hainline et al. 2011; Ivison et al. 2011; Wardlow et al. 2011). There are a number of methods that can be used to identify AGN activity, including X-ray

emission (Alexander et al. 2003), mid-IR colour selection (Ivison et al. 2004), mid-IR spectral properties (Valiante et al. 2007; Menéndez-Delmestre et al. 2009) and optical spectral properties (Swinbank et al. 2004). Hainline et al. (2011) analysed a sample of X-ray-observed SMGs, finding that the fractional contribution to the mid-IR from non-stellar (i.e. power-law) emission provides an excellent proxy for the hard X-ray luminosity and so provides a robust AGN diagnostic.

We have compiled the AGN classifications for our sample: we find that 13/40 SMGs in our sample have been observed to have AGN activity, based on one (or more) of the above diagnostics. It must be noted, however, that the selection of the C05 sample could result in a bias towards SMGs containing AGN, as a result radio pre-selection, and/or the presence of strong emission lines in their rest-frame UV spectra (this is discussed in Hainline et al. 2011; see also Wardlow et al. 2011). If this is the case, then our sample – being substantially drawn from the C05 sample – could also be biased towards a higher percentage of AGN than the general SMG population. Nevertheless, we can still use our sample to investigate the correlation between the presence of an AGN and its luminosity, with other physical properties of the SMG hosts.

In fact, we find little or no correlation between the presence of an actively fuelled SMBH, shown by AGN activity, and the ^{12}CO properties of the SMGs in our sample: gas masses, gas fractions and FWHM-derived dynamical masses for the AGN-hosting subsample are all consistent with being identical to the ^{12}CO sample as a whole. This is in-line with the picture that SMGs are star formation dominated, with activity from a central AGN playing little part in determining the properties of the system. Indeed, it implies that the AGN activity occurs in all classes of SMGs, irrespective of dynamical or gas masses. The lack of any difference in the gas fractions of the SMGs showing AGN activity and those without, may be indicating that any feedback effect from the AGN influences both the dust and gas reservoirs in these galaxies. In this way, those 'evolved' systems where the AGN have had the most influence would no longer appear in our 850-μm-selected SMG sample due to an increase in dust temperature or a reduction in cold dust mass.

5.2 The $M_{BH}-\sigma$ relation

SMGs have been proposed as the precursors of the massive ellipticals seen in the local Universe (e.g. Swinbank et al. 2006; Hickox et al. 2012). This population also exhibit the tightest $M_{BH}-\sigma$ relation (Gültekin et al. 2009), and as such examining their $M_{BH}-\sigma$ connection during the time of their peak star formation activity may be useful if we are to understand the role of feedback in the galaxy formation process. Unfortunately, one difficulty with addressing the evolution of the $M_{BH}-\sigma$ relation in SMGs using direct kinematic measures is the fact that observations of the central stellar velocity dispersions at high redshift are not possible with the current generation of telescopes. Similarly, use of optical and near-IR emission line gas as a tracer of host galaxy dynamics is complicated by the mixture of obscuration and potential outflow in these systems (e.g. Swinbank et al. 2006; Alexander et al. 2010). Previous attempts to study the $M_{BH}-\sigma$ relation in SMGs have therefore been forced to use estimates of the stellar and gas masses as a proxy for σ of the host galaxy (Alexander et al. 2005, 2008; Borys et al. 2005). These studies uncovered an apparent offset between the relation for SMGs and that seen for spheroids at $z \sim 0$, in the sense that the SMBH masses were lower in the SMGs, relative to the host galaxy mass. This behaviour is the reverse of that seen in studies of the SMBHs in QSOs (Peng et al. 2006), including those using ^{12}CO

dynamics (Walter et al. 2004; Coppin et al. 2008; Simpson et al. 2012), suggesting that SMGs must grow their SMBHs to lie on the present-day relation.

Our large sample of SMGs with ^{12}CO observations (providing well-constrained individual baryonic masses and robust kinematic information) is also a useful tool for analysing the relationship of the mass of the SMBH to that of their galaxy hosts, and compare this to the present-day $M_{BH}-\sigma$ relation to search for evolutionary changes. We therefore start by estimating the SMBH masses for the SMGs following Alexander et al. (2005b). We derive SMBH masses from the X-ray luminosity integrated from 0.5 to 8 keV (Alexander et al. 2003), assuming that the X-ray emission from the AGN accounts for 6^{+12}_{-4} per cent of its total bolometric luminosity (Elvis et al. 1994). Next, an 'Eddington ratio', η, can be adopted, which is the ratio of the AGN bolometric luminosity to the Eddington luminosity. As the Eddington luminosity is simply a function of black hole (BH) mass, this allows us to estimate the mass of the central SMBH. Of course, the adoption of an assumed Eddington ratio is a critical step here, and a source of uncertainty. Alexander et al. (2008) investigated a sample of SMGs taken from the parent sample of C05, and estimate a typical value for the Eddington ratio of $\eta = 0.2$–0.5.[6] Here, we adopt a value of $\eta = 0.4^{+0.1}_{-0.2}$, and include the uncertainty in η in the resulting uncertainty on the derived SMBH masses.

We then derive the equivalent velocity dispersion of the galaxy from our ^{12}CO linewidths, using the prescription of Ho (2007):

$$\log_{10} \sigma = (1.26 \pm 0.05)\log\left(\frac{V_{20}}{2}\right) - (0.78 \pm 0.11), \quad (13)$$

where $\sigma_\star$ is the stellar velocity dispersion of the bulge, and V_{20} is the velocity width at 20 per cent of the peak. This can be somewhat uncertain for lower luminosity galaxies (and, of course, varies for sources with non-Gaussian emission profiles), but for IR-bright galaxies ($L_{IR} \sim 10^{12}$ L$_\odot$) such as our SMGs the relationship between V_{20} and FWHM ($=V_{50}$) approaches the analytic relation for a Gaussian profile, $V_{20} \simeq 1.5 \times$ FWHM (Ho 2007).

Fig. 10 shows σ versus L_X (and the resulting derived values of M_{BH} and M_{dyn}) for our sample of SMGs, which have been coded according to their baryonic gas fraction. Included in the plot are local elliptical galaxies (thought to be the low-redshifts decedents of SMGs), as well as a fit to the local data (Gültekin et al. 2009). The SMGs in our sample lie below the local $M_{BH}-\sigma$ relationship, with SMBH masses approximately an order of magnitude lower than would be predicted based on their dynamical properties. This confirms the offset previously seen for SMGs using indirect estimates of their masses (e.g. Borys et al. 2005; Alexander et al. 2008).

As discussed by Alexander et al. (2008), if we wished to remove this offset from the local $M_{BH}-\sigma$ by adopting a lower Eddington Ratio, we would be forced to an extremely low value of $\eta \sim 0.05$. This would imply an unfeasibly slow SMBH growth rate during a phase where the necessary gas supply should be abundant (though on short time-scales there could be a temporary dearth of gas surrounding the central BH). We conclude that SMGs represent a population which has yet to evolve on to the low-redshift $M_{BH}-\sigma$ relation. While their high FWHMs (especially in the high-J_{up} lines, which trace the compact, central potentials) are indicative of massive galaxies, the central SMBHs are still relatively immature, having yet to grow substantially due to rapid mass accretion.

---

[6] This range in estimations of η is primarily driven by the unknown distribution of gas within the broad-line region of the BH.
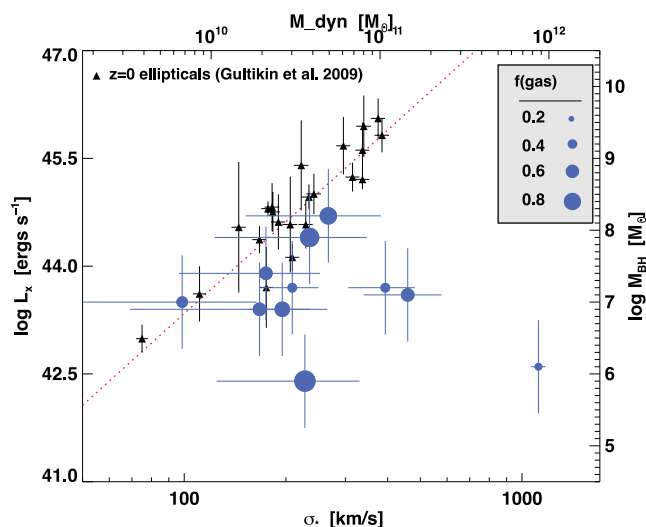
Figure 10. The $M_{BH}-\sigma_*$ relation for the SMGs in our sample with measured X-ray luminosities, which have been converted into SMBH masses following Alexander et al. (2005). We also plot the same quantities for local elliptical galaxies, as presented by Gültekin et al. (2009), and the best-fitting relation from the same work (with a slope $\beta = 4.24$). The SMGs have SMBH masses almost an order of magnitude lower than their dynamical properties would suggest, suggesting that they represent a population yet to evolve on to the $M_{BH}-\sigma$ relation. The size of the SMG points scales with the baryonic gas fraction, two examples of which are shown in the key. There is no correlation between gas fraction and position in the diagram, suggesting that the rapid SMBH 'feeding' stage may occur after the starburst episode.

An SMG's position in the $M_{BH}-\sigma$ plane may evolve with age, as the central SMBH accretes mass and the gas is turned into stars. A low baryonic gas fraction could be interpreted as a sign that the SMG is a 'more evolved' spheroid towards the end of the starburst episode, having already converted much of its gas reservoir into stars. As a result, if the SMBH growth occurs concomitantly with the starburst phase, we might expect gas fractions to correlate inversely with the ratio of SMBH to dynamical mass. As we see in Fig. 10, there is no apparent trend for lower f_{gas} SMGs to be closer to the present-day $M_{BH}-\sigma$ relation, although the small number of SMGs and the significant scatter which may be present in σ due to geometrical projection, weaken the strength of any conclusions. Equally, the lack of any apparent correlation may suggest that the rapid BH 'feeding' stage occurs separately, after the starburst episode which causes the galaxies to be sub-mm selected. Indeed, the time-scales required to grow the SMBHs to the point that they resemble those of their $z \sim 0$ counterparts (which have $M_{BH} \gtrsim 4 \times 10^8$ M$_\odot$; Alexander et al. 2008) are significantly longer than the expected sub-mm-bright lifetime (100–300 Myr; Swinbank et al. 2006; Hickox et al. 2012), again indicating the need for a subsequent phase of predominantly SMBH growth, most likely associated with strong AGN activity. Interferometric observations of far-IR-bright QSOs could be a way to approach this phase from the 'other side', potentially shedding light on this interesting problem (Simpson et al. 2012 – see also Walter et al. 2004; Riechers et al. 2008).

6 CONCLUSIONS

We have presented results from a large PdBI survey for molecular gas in luminous SMGs. We observed 40 SMGs with well-defined redshifts, detecting ^{12}CO emission in 32. For the remaining eight

SMGs without detected ^{12}CO emission, we constrain the upper limits on their ^{12}CO flux. We used gas masses and dynamical masses from our sample, combined with ancillary multiwavelength data (including far-IR luminosities and stellar masses), to discuss the physical properties of the SMG population. Our main conclusions are as follows.

(i) Analysing the median ^{12}CO SLED for our SMG sample, after normalization to a mean far-IR luminosity, we find that the SLED rises up to $J_{up} \sim 5$. Data are sparse at $J_{up} > 5$, but within the errors we find evidence for a turnover.

(ii) Plotting ^{12}CO luminosity against linewidth, we find that $L'_{CO(1-0)} \propto \sigma^2$ is a good fit to the trend seen in our sample. The scatter around this relation is lower than would be expected for a population of randomly oriented discs. This suggests that the ISM in luminous SMGs typically exists as a thick disc or turbulent ellipsoid.

(iii) The ^{12}CO linewidths are, in general, broad, having a mean FWHM of 510 ± 80 km s^{-1}. Using these linewidths, we derive dynamical masses and find mean values – for virial and rotational mass estimators – of $(7.1 \pm 1.0) \times 10^{10}$ and $(1.6 \pm 0.3) \times 10^{10}$ R_{kpc} M$_\odot$, respectively. In these calculations, we have kept the dependence on the size of the ^{12}CO reservoir, which is not well constrained for the majority of our sources. We also find that 20–28 per cent of the sample exhibit double-peaked ^{12}CO profiles, which we interpret as a signature of an on-going merger.

(iv) We use far-IR luminosities to assess the SFE in our SMGs. While we find an approximately linear slope to the $L'_{CO(1-0)}-L_{FIR}$ relation, without brightness temperature ratio measurements for individual sources this result is uncertain, and we suggest that it is difficult to draw any strong conclusions about the gas depletion time-scales of the different populations from high-J_{up} observations.

(v) We see little evidence of evolution in the baryonic gas fraction in SMGs with redshift. The median value for our sample is 40–60 per cent at all redshifts. By comparison to recently derived gas fractions for other high-redshift populations, we conclude that SMGs do not have significantly higher gas fractions than more modestly SMGs at similar redshifts.

(vi) We compile a variety of archival multiwavelength data in order to analyse the AGN contribution to the SMG population as a whole. We find that 30 per cent of our sample have some indication of AGN activity, but the presence of an AGN does not seem to have a significant effect on the gas properties of the host SMG. We also make use of deep X-ray data to estimate SMBH masses for our SMGs. We find that the SMBHs in SMGs lie substantially below the $z \sim 0$ $M_{BH}-\sigma$ relation, and that there is no correlation between SMG gas fraction and SMBH mass. We conclude that the SMBH growth phase occurs separately from, and after, the 'star formation' phase, which our sample of SMGs is undergoing.

REFERENCES

Alaghband-Zadeh S. et al., 2012, MNRAS, 424, 2232

Alexander D. M. et al., 2003, AJ, 125, 383

Alexander D. M., Smail I., Bauer F. E., Chapman S. C., Blain A. W., Brandt W. N., Ivison R. J., 2005a, Nat, 434, 738

Alexander D. M., Bauer F. E., Chapman S. C., Smail I., Blain A. W., Brandt W. N., Ivison R. J., 2005b, ApJ, 632, 736

Alexander D. M. et al., 2008, AJ, 135, 1968

Alexander D. M., Swinbank A. M., Smail I., McDermid R., Nesvadba N. P. H., 2010, MNRAS, 402, 2211

Banerji M., Chapman S. C., Smail I., Alaghband-Zadeh S., Swinbank A. M., Dunlop J. S., Ivison R. J., Blain A. W., 2011, MNRAS, 418, 1071

Barger A. J., Wang W.-H., Cowie L. L., Owen F. N., Chen C.-C., Williams J. P., 2012, ApJ, 761, 89

Baugh C. M., Lacey C. G., Frenk C. S., Granato G. L., Silva L., Bressan A., Benson A. J., Cole S., 2005, MNRAS, 356, 1191

Benson A. J., Bower R. G., Frenk C. S., Lacey C. G., Baugh C. M., Cole S., 2003, ApJ, 599, 38

Bertoldi F., Menten K. M., Kreysa E., Carilli C. L., Owen F., 2002, HiA, 12, 473

Biggs A. D., Ivison R. J., 2006, MNRAS, 371, 963

Biggs A. D. et al., 2011, MNRAS, 413, 2314

Blain A. W., Kneib J., Ivison R. J., Smail I., 1999, ApJ, 512, L87

Bolatto A. D. et al., 2011, ApJ, 741, 12

Borys C., Smail I., Chapman S. C., Blain A. W., Alexander D. M., Ivison R. J., 2005, ApJ, 635, 853

Bothwell M. S., Kennicutt R. C., Lee J. C., 2009, MNRAS, 400, 154

Bothwell M. S. et al., 2010, MNRAS, 405, 219

Carilli C. L. et al., 2010, ApJ, 714, 1407

Casey C. M. et al., 2009a, MNRAS, 399, 121

Casey C. M. et al., 2009b, MNRAS, 400, 670

Casey C. M. et al., 2011, MNRAS, 415, 2723

Casey C. M., 2012, MNRAS, 425, 3094

Chabrier G., 2003, PASP, 115, 763

Chapman S. C. et al., 2001, ApJ, 648, 147

Chapman S. C., Smail I., Ivison R. J., Helou G., Dale D. A., Lagache G., 2002, ApJ, 573, 66

Chapman S. C., Blain A. W., Ivison R. J., Smail I. R., 2003, Nat, 422, 695

Chapman S. C., Smail I., Blain A. W., Ivison R. J., 2004, ApJ, 614, 671

Chapman S. C., Blain A. W., Smail I., Ivison R. J., 2005, ApJ, 622, 772 (C05)

Chapman S. C. et al., 2008, ApJ, 689, 889

Chapman S. C. et al., 2010, MNRAS, 409, L13

Coppin K. E. K. et al., 2006, MNRAS, 372, 1621

Coppin K. E. K. et al., 2008, MNRAS, 389, 45

Coppin K. E. K. et al., 2010, MNRAS, 407, L103

Crosthwaite L. P., Turner J. L., 2007, AJ, 134, 1827

Daddi E. et al., 2007, ApJ, 670, 156

Daddi E., Dannerbauer H., Krips M., Walter F., Dickinson M., Elbaz D., Morrison G. E., 2009, ApJ, 695, L176

Daddi E. et al., 2010, ApJ, 713, 686

Danielson A. L. R. et al., 2011, MNRAS, 410, 1687

Dannerbauer H., Daddi E., Riechers D. A., Walter F., Carilli C. L., Dickinson M., Elbaz D., Morrison G. E., 2009, ApJ, 698, L178

Davé R., Finlator K., Oppenheimer B. D., 2011, MNRAS, 416, 1354

Downes D., Solomon P. M., 1998, ApJ, 507, 1615

Elvis M. et al., 1994, ApJS, 95, 1

Engel H. et al., 2010, ApJ, 724, 233

Erb D. K., Steidel C. C., Shapley A. E., Pettini M., Reddy N. A., Adelberger K. L., 2006, ApJ, 646, 107

Ferrarese L., Merritt D., 2000, ApJ, 539, L9

Förster Schreiber N. M. et al., 2006, ApJ, 645, 1062

Frayer D. T., Ivison R. J., Scoville N. Z., Yun M., Evans A. S., Smail I., Blain A. W., Kneib J.-P., 1998, ApJ, 506, L7

Frayer D. T. et al., 1999, ApJ, 514, L13

Geach J. E., Smail I., Moran S. M., MacArthur L. A., Lagos C. d. P., Edge A. C., 2011, ApJ, 730, L19

Genzel R., Baker A. J., Tacconi L. J., Lutz D., Cox P., Guilloteau S., Omont A., 2003, ApJ, 584, 633

Genzel R. et al., 2010, MNRAS, 407, 2091

Genzel R. et al., 2012, ApJ, 746, 69

Greve T. R., Ivison R. J., Bertoldi F., Stevens J. A., Dunlop J. S., Lutz D., Carilli C. L., 2004, MNRAS, 354, 779

Greve T. R. et al., 2005, MNRAS, 359, 1165

Gültekin K. et al., 2009, ApJ, 698, 198

Hainline L. J., Blain A. W., Smail I., Frayer D. T., Chapman S. C., Ivison R. J., Alexander D. M., 2009, ApJ, 699, 1610

Hainline L. J., Blain A. W., Smail I., Alexander D. M., Armus L., Chapman S. C., Ivison R. J., 2011, ApJ, 740, 96

Harris A. I., Baker A. J., Zonak S. G., Sharon C. E., Genzel R., Rauch K., Watts G., Creager R., 2010, ApJ, 723, 1139

Hickox R. C. et al., 2012, MNRAS, 421, 284

Hill M. D., Shanks T., 2011, MNRAS, 410, 762

Ho L. C., 2007, ApJ, 669, 821

Holland et al., 1999, MNRAS, 303, 659

Hopkins A. M., Beacom J. F., 2006, ApJ, 651, 142

Ivison R. J., Smail I., Le Borgne J.-F., Blain A. W., Kneib J.-P., Bezecourt J., Kerr T. H., Davies J. K., 1998, MNRAS, 298, 583

Ivison R. J., Smail I., Frayer D. T., Kneib J.-P., Blain A. W., 2001, ApJ, 561, L45

Ivison R. J. et al., 2004, ApJS, 154, 124

Ivison R. J., Smail I., Papadopoulos P. P., Wold I., Richard J., Swinbank A. M., Kneib J.-P., Owen F. N., 2010, MNRAS, 404, 198

Ivison R. J., Papadopoulos P. P., Smail I., Greve T. R., Thomson A. P., Xilouris E. M., Chapman S. C., 2011, MNRAS, 412, 1913

Karim A. et al., 2011, ApJ, 730, 61

Karim A. et al., 2012, arXiv:1210:0249

Krumholz M. R., Dekel A., 2012, ApJ, 753, 16

Lagos C. D. P., Baugh C. M., Lacey C. G., Benson A. J., Kim H.-S., Power C., 2011, MNRAS, 418, 1649

Law D. R., Steidel C. C., Erb D. K., Larkin J. E., Pettini M., Shapley A. E., Wright S. A., 2009, ApJ, 697, 2057

Ledlow M. J., Smail I., Owen F. N., Keel W. C., Ivison R. J., Morrison G. E., 2002, ApJ, 577, L79

Liszt H. S., Pety J., Lucas R., 2010, A&A, 518, A45

Lutz D. et al., 2010, ApJ, 712, 1287

Magnelli B. et al., 2010, A&A, 518, L28

Magnelli B. et al., 2012, A&A, 539, A155

Magorrian J. et al., 1998, AJ, 115, 2285

Meijerink R., Spaans M., Israel F. P., 2007, A&A, 461, 793

Menéndez-Delmestre K. et al., 2009, ApJ, 699, 667

Narayanan D., Hayward C. C., Cox T. J., Hernquist L., Jonsson P., Younger J. D., Groves B., 2010, MNRAS, 401, 1613

Narayanan D., Krumholz M., Ostriker E. C., Hernquist L., 2011, MNRAS, 418, 664

Neri R. et al., 2003, ApJ, 597, L113

Noeske K. G. et al., 2007, ApJ, 660, L47

Papadopoulos P. P., van der Werf P., Xilouris E., Isaak K. G., Gao Y., 2012, ApJ, 758, 71

Papovich C., Finkelstein S. L., Ferguson H. C., Lotz J. M., Giavalisco M., 2011, MNRAS, 412, 1123

Peng C. Y., Impey C. D., Rix H.-W., Kochanek C. S., Keeton C. R., Falco E. E., Lehár J., McLeod B. A., 2006, ApJ, 649, 616

Pope A. et al., 2006, MNRAS, 370, 1185

Pope A. et al., 2008, ApJ, 675, 1171

Riechers D. A., Walter F., Brewer B. J., Carilli C. L., Lewis G. F., Bertoldi F., Cox P., 2008, ApJ, 686, 851

Riechers D. A. et al., 2010, ApJ, 720, L131

Riechers D. A., Hodge J., Walter F., Carilli C. L., Bertoldi F., 2011, ApJ, 739, L31

Rodighiero G. et al., 2010, A&A, 518, L25

Sanders D. B., Scoville N. Z., Soifer B. T., 1991, ApJ, 370, 158

Schiminovich D., Wyder T. K., Martin D. C., Johnson B. D., 2007, ApJS, 173, 315

Schinnerer E. et al., 2008, ApJ, 689, L5

Shapiro K. L. et al., 2009, ApJ, 701, 955

Simpson J. M. et al., 2012, MNRAS, 426, 3201

Smail I., Ivison R. J., Blain A. W., 1997, ApJ, 490, L5

Smail I., Ivison R. J., Blain A. W., Kneib J. P., 2002, MNRAS, 331, 495

Sobral D., Best P., Smail I., Geach J., Hizels Team, 2011, in Wang W., Lu J., Luo Z., Yang Z., Hua H., Chen Z., eds, ASP Conf. Ser. Vol. 446, The Nature and Evolution of Hα Emitters at High-z with HiZELS. Astron. Soc. Pac., San Francisco, p. 249

Sobral D., Smail I., Best P. N., Geach J. E., Matsuda Y., Stott J. P., Cirasuolo M., Kurk J., 2013, MNRAS, 428, 1128

Solomon P. M., Vanden Bout P. A., 2005, ARAA, 43, 677

Solomon P. M., Downes D., Radford S. J. E., Barrett J. W., 1997, ApJ, 478, 144

Swinbank A. M., Smail I., Chapman S. C., Blain A. W., Ivison R. J., Keel W. C., 2004, ApJ, 617, 64

Swinbank A. M., Chapman S. C., Smail I., Lindner C., Borys C., Blain A. W., Ivison R. J., Lewis G. F., 2006, MNRAS, 371, 465

Swinbank A. M. et al., 2008, MNRAS, 391, 420

Swinbank A. M. et al., 2010, MNRAS, 405, 234

Swinbank A. M. et al., 2011, ApJ, 742, 11

Tacconi L. J. et al., 2006, ApJ, 640, 228

Tacconi L. J. et al., 2008, ApJ, 680, 246

Tacconi L. J. et al., 2010, Nat, 463, 781

Valiante E., Lutz D., Sturm E., Genzel R., Tacconi L. J., Lehnert M. D., Baker A. J., 2007, ApJ, 660, 1060

Vieira J. D. et al., 2010, ApJ, 719, 763

Walter F., Carilli C., Daddi E., 2011, in von Berlepsch R., ed., Reviews in Modern Astronomy. Wiley-VCH, Berlin, p. 167

Walter F., Carilli C., Bertoldi F., Menten K., Cox P., Lo K. Y., Fan X., Strauss M. A., 2004, ApJ, 615, L17

Wang W.-H., Cowie L. L., Barger A. J., Williams J. P., 2011, ApJ, 726, L18

Wardlow J. L. et al., 2011, MNRAS, 415, 1479

Weiss A., Downes D., Walter F., Henkel C., 2007, in Baker A. J., Glenn J., Harris A. I., Mangum J. G., Yun M. S., eds, ASP Conf. Ser. Vol. 375, From Z-Machines to ALMA: (Sub)Millimeter Spectroscopy of Galaxies. Astron. Soc. Pac., San Francisco, p. 25

Young J. S., Scoville N. Z., 1991, ARA&A, 29, 581

Yun M. S., Reddy N. A., Condon J. J., 2001, ApJ, 554, 803

SUPPORTING INFORMATION

Additional Supporting Information may be found in the online version of this article:

Appendix A.
Appendix B.
(http://mnras.oxfordjournals.org/lookup/suppl/doi:10.1093/mnras/sts562/-/DC1).

Please note: Oxford University Press are not responsible for the content or functionality of any supporting materials supplied by the authors. Any queries (other than missing material) should be directed to the corresponding author for the article.

This paper has been typeset from a TEX/LATEX file prepared by the author.